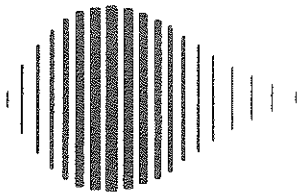

NATIONAL CENTER FOR EARTHQUAKE
ENGINEERING RESEARCH
State University of New York at Buffalo

EXPERIMENT ON PERFORMANCE OF BURIED PIPELINES ACROSS SAN ANDREAS FAULT

by

J. Isenberg and E. Richardson
Weidlinger Associates
4410 El Camino Real, Suite 110
Los Altos, California 94022

and

T. D. O'Rourke
Department of Structural Engineering
School of Civil and Environmental Engineering
Cornell University
Ithaca, New York 14853

Technical Report NCEER-89-0005

March 10, 1989

This research was conducted at Weidlinger Associates and Cornell University and was partially supported by the National Science Foundation under Grant No. ECE 86-07591.

NOTICE

This report was prepared by Weidlinger Associates and Cornell University as a result of research sponsored by the National Center for Earthquake Engineering Research (NCEER). Neither NCEER, associates of NCEER, its sponsors, Weidlinger Associates, Cornell University or any person acting on their behalf:

a. makes any warranty, express or implied, with respect to the use of any information, apparatus, method, or process disclosed in this report or that such use may not infringe upon privately owned rights; or

b. assumes any liabilities of whatsoever kind with respect to the use of, or the damage resulting from the use of, any information, apparatus, method or process disclosed in this report.

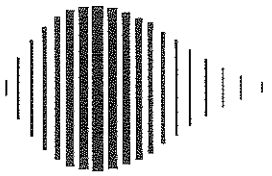

EXPERIMENT ON PERFORMANCE OF BURIED PIPELINES ACROSS SAN ANDREAS FAULT

by

J. Isenberg,[1] E. Richardson[2] and T.D. O'Rourke[3]

March 10, 1989

Technical Report NCEER-89-0005

NCEER Contract Number 87-3001

NSF Master Contract Number ECE 86-07591

1 Principal, Weidlinger Associates, Los Altos, California
2 Associate, Weidlinger Associates, Los Altos, California
3 Professor, Dept. of Structural Engineering, School of Civil and Environmental Engineering, Cornell University

NATIONAL CENTER FOR EARTHQUAKE ENGINEERING RESEARCH
State University of New York at Buffalo
Red Jacket Quadrangle, Buffalo, NY 14261

PREFACE

The National Center for Earthquake Engineering Research (NCEER) is devoted to the expansion and dissemination of knowledge about earthquakes, the improvement of earthquake-resistant design, and the implementation of seismic hazard mitigation procedures to minimize loss of lives and property. The emphasis is on structures and lifelines that are found in zones of moderate to high seismicity throughout the United States.

NCEER's research is being carried out in an integrated and coordinated manner following a structured program. The current research program comprises four main areas:

- Existing and New Structures
- Secondary and Protective Systems
- Lifeline Systems
- Disaster Research and Planning

This technical report pertains to Program 3, Lifeline Systems, and more specifically to water delivery systems.

The safe and serviceable operation of lifeline systems such as gas, electricity, oil, water, communication and transportation networks, immediately after a severe earthquake, is of crucial importance to the welfare of the general public, and to the mitigation of seismic hazards upon society at large. The long-term goals of the lifeline study are to evaluate the seismic performance of lifeline systems in general, and to recommend measures for mitigating the societal risk arising from their failures.

From this point of view, Center researchers are concentrating on the study of specific existing lifeline systems, such as water delivery and crude oil transmission systems. The water delivery system study consists of two parts. The first studies the seismic performance of water delivery systems on the west coast, while the second addresses itself to the seismic performance of the water delivery system in Memphis, Tennessee. For both systems, post-earthquake fire fighting capabilities will be considered as a measure of seismic performance.

The components of the water delivery system study are shown in the accompanying figure.

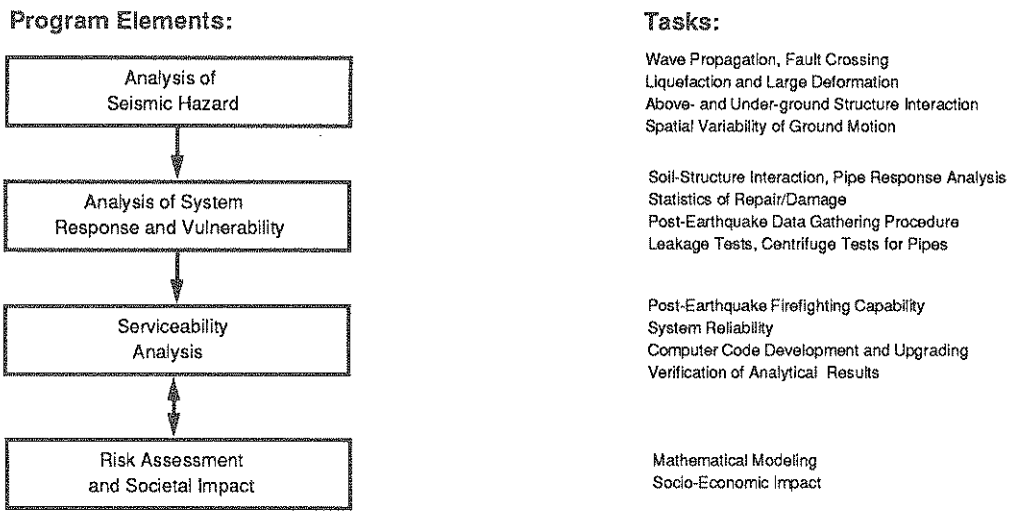

This report describes the status of a field experiment designed to investigate the performance of buried pipelines at a fault crossing during an earthquake. The experiment is in place in Owen's Pasture near Parkfield, California. This past year, researchers have added strong motion seismometers and survey monuments to the site, and plan to continue to upgrade instrumentation to improve measurement techniques. The experiment will remain in place until the occurrence of an earthquake.

ABSTRACT

A field experiment designed to investigate the performance of buried pipelines at a fault crossing has been constructed near Parkfield, CA. The site was chosen to capitalize on the predicted recurrence of the 1966 Parkfield-Cholame earthquake sequence. Monuments for measuring lateral offset and strong motion seismometers have been placed at the site and are being monitored. Thirty six strain gages have been attached to two segments of welded steel pipe to measure length changes and flexure. Twelve displacement transducers have been installed in jointed ductile iron pipe to measure rotation and extension at the joints. Data are recorded when preassigned threshold levels of strain in selected trigger channels are exceeded. Since seismic activity has been low, no records of pipeline response have been obtained yet.

The accomplishments of 1988 include measuring the stress-strain properties of the pipeline steel and shear strength of the interface between sand and steel. Three strong motion seismometers, obtained through a cooperative agreement with the Urban Hazards Research Institute of the University of Kyoto, Japan, were put in place. Survey monuments were also emplaced and are monitored regularly by the US Geological Survey. The concrete anchors which are intended to prevent relative displacement between the pipe and the adjacent soil at the ends of the welded steel pipes were enlarged.

Future work includes upgrading the data acquisition rate such that the strain measurements and ground strains derived from the seismometers are both resolved up to 8-10 Hz; and further reducing noise in a few strain gage channels.

TABLE OF CONTENTS

LIST OF FIGURES

LIST OF TABLES

SECTION 1
INTRODUCTION

In July 1987, an experimental facility to study the seismic response of buried pipelines was constructed near Parkfield, CA, Refs. 1 and 2. This experiment is designed to capitalize on the predicted recurrence of the 1966 Parkfield-Cholame earthquake sequence by placing buried pipeline segments across a strand of the San Andreas Fault. The specific location is Owen's Pasture, about 2 km West Northwest from the town of Parkfield, where surface rupture was observed during the 1966 earthquake and where surface creep is currently being measured by USGS creepmeter XPK1 at an average rate of about 13 mm per year.

Many high pressure pipelines are constructed with continuous girth-welded steel sections of pipe. The inherent ductility of steel makes these types of pipelines well suited to sustain plastic strain if deformed in tension. An original aim of the experiment was to provide data for evaluating analytical models (Refs. 3 and 4) which account for tensile deformation of continuous pipelines at fault crossings. It should be recognized that such models are not necessarily confined to fault movement, but also can apply, in certain instances, to ground ruptures at the margins of lateral spreads or earthquake-induced landslides.

Figures 1-1a and 1-1b show a plan view of a pipeline which is intersected by a right lateral strike-slip fault at an angle, β. The pipeline is oriented so that fault displacement, d_f, will cause tension in the buried pipeline. Newmark and Hall (Ref. 3) analyzed the pipeline deformation as an axisymmetric pattern of circular arcs, with each circular segment spanning the fault centerline and the location of an anchor point. The distance between the fault and the anchor point is known as the anchor length, L_a. Anchors may be caused by bends, tie-ins, and other features which develop substantial resistance to axial movement. Alternatively, the anchor point may represent an effective anchor length, beyond which there is no axial stress imposed in the pipeline from fault movement. As originally proposed, the Newmark-Hall model accounts for the stress-strain response of the pipeline steel as a bi- or tri-linear relationship.

The analytical model developed by Kennedy, et al. (Ref. 4) accounts for the concentration of pipeline bending near the fault trace, increased frictional resistance between the pipe and soil in the zone of maximum bending, and the nonlinear response of the pipeline steel to large tensile deformation. As illustrated in Fig. 1-1c, the zone of increased frictional resistance is assumed to conform with the zone of pipeline curvature. As in the Newmark-Hall model, Kennedy, et al.

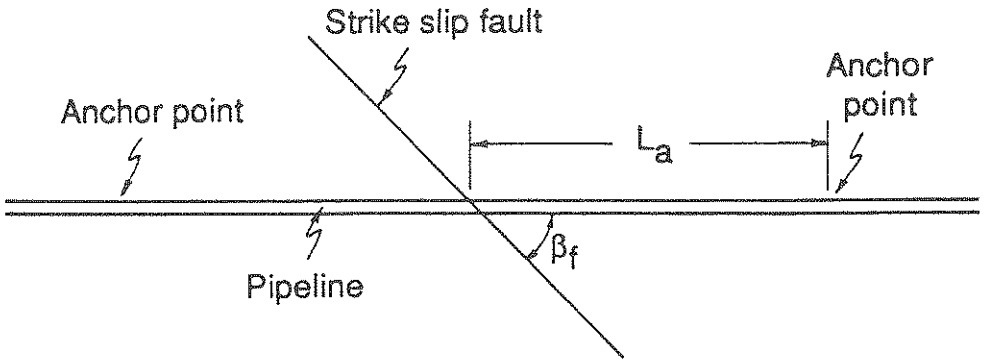

a) Before Fault Movement

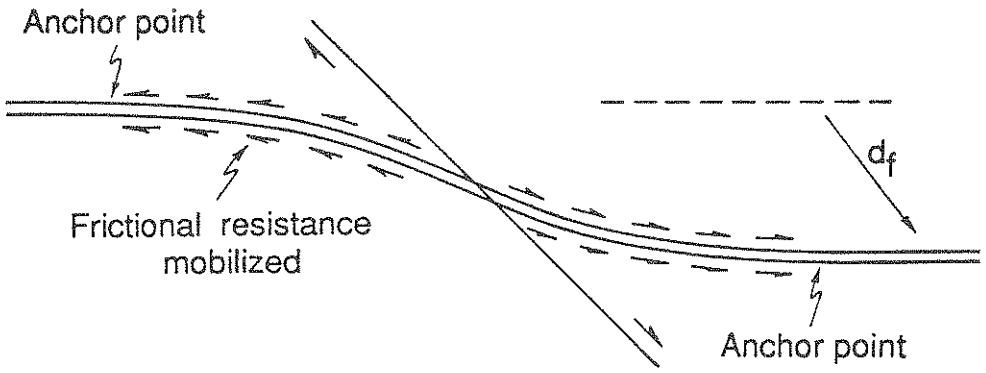

b) After Fault Movement

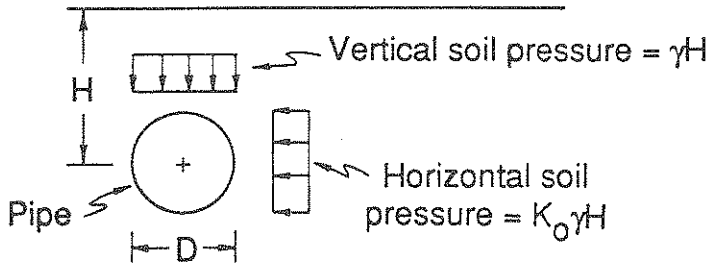

c) Transverse Cross-Section

FIGURE 1-1 Plan And Sectional Views Of Continuous Pipeline Envisioned In Newmark-Hall Design Approach

assumed that the pipeline deforms in an axisymmetric pattern of two circular arcs, with longitudinal shear stresses mobilized along the pipeline to the location of an actual or effective anchor point.

The assumptions embodied in these models and others, of which Ref. 5 is representative, including friction at the pipe-soil interface and coefficients of passive soil resistance, have been partially investigated under laboratory conditions (Refs. 6 and 7), but cannot be studied fully in the laboratory on account of the difficulty in creating appropriate boundary conditions. The present experiment aims to overcome some of the problems associated with boundary conditions by using sections of pipe which are long enough to develop bending and longitudinal strains representative of field conditions. Even though the welded steel segments of the experimental pipelines are 200 ft long, it is still necessary to restrain the ends by means of large concrete anchors in order to prevent axial displacement at the ends, and thus ensure that the end conditions of the pipe are precisely defined.

To investigate the behavior of pipelines intersected by surface ruptures and to provide data for evaluating design and analysis methods for the deformation mode shown in Fig. 1-1, continuously welded steel pipe and jointed ductile iron pipe segments were instrumented with strain gages and displacement transducers, respectively, and buried at the Owen's Pasture site. Automatic recording of data capable of resolving deformations with a maximum frequency of 1 hz was established. A line of monuments was placed across the assumed location of the eventual surface rupture to measure lateral offset during both pre-earthquake creep and earthquake-induced surface rupture phases.

During 1988, the aim of the experiment was expanded to include the effects of ground shaking caused by wave propagation. Mathematical models have also been proposed to support the design of pipelines exposed to shaking, Refs. 8 through 12. Figure 1-2 illustrates the interaction of a pipe segment with an obliquely incident train of waves. A common assumption of such models is that the ground deformation is due to a wave train propagating with a predominant wave length and group velocity, and is imposed on the pipeline with deformation and, in some cases, damping of the soil considered. The dynamic pipe-soil interaction is assumed to be negligible. Field experiments to investigate the relationship between ground shaking and the response of continuous pipelines are also being conducted in Tokyo at a site where surface rupture is not expected, Ref. 13. The Parkfield experiment, which complements the Japanese work, measures ground shaking close to the expected zone of surface rupture by means of three seismometers which were contributed to the project by Prof. H. Kameda, Director of the Urban Hazards Research Institute at Kyoto University.

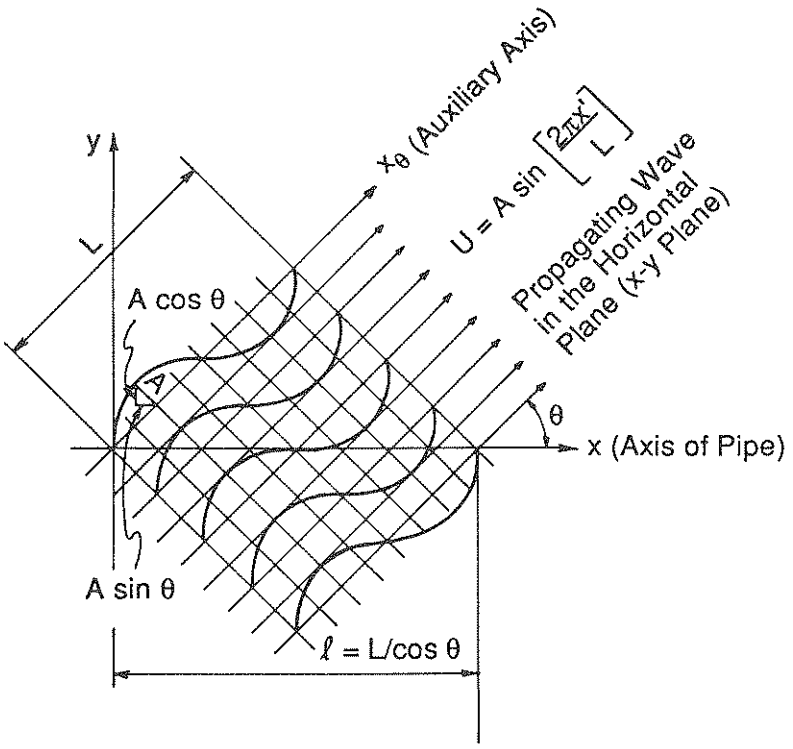

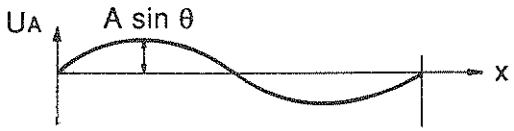

Axial Displacement
(in x - Direction)

Displacement: $U_A = A \sin\theta \cdot \sin\left[\frac{2\pi \cos\theta}{L} \cdot x\right]$

Strain: $\frac{dU_A}{dx} = \frac{2\pi A}{L} \sin\varnothing \cdot \cos\varnothing \cos\left[\frac{2\pi \cos\theta}{L} x\right]$

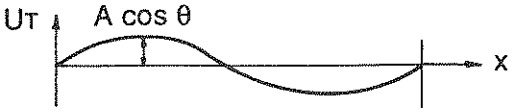

Transverse Displacement
(in y - Direction)

Displacement: $Ur = A \cos\varnothing \cdot \sin\left[\frac{2\pi \cos\varnothing}{L}\right]$

Curvature: $\varnothing = \frac{d^2Ur}{dx^2} = \frac{-4\pi^2 A}{L^2} \cos^3\varnothing \cdot \sin\left[\frac{2\pi \cos\theta}{L} x\right]$

FIGURE 1-2 Model Of Wave Propagation Effects For Pipeline Analysis (After Ref.20)

Seismic surveillance continues in the Parkfield area through a widespread system of measurement and recording devices. As of the date of this report, the predicted Magnitude 6.0 earthquake has not occurred. There have been some premonitory events, such as microearthquake swarms, outgassing from wells or accelerated rates of creep, since September 1987 when the last report under the present project was published. The US Geological Survey, which conducts the Parkfield Prediction Project, is continuing to monitor instruments within the Parkfield Box and publishes a monthly update of findings. There is no evidence that the seismic activity which has occurred recently in California has had any effect on the locked or creeping segments of the San Andreas Fault near Parkfield.

With regard to the pipeline experiment, the welded steel pipe segments were instrumented with 36 strain gages and two temperature sensors. The ductile iron pipes were instrumented with 12 transducers, and all segments were buried by October 1987. The cables were attached to the data logger and automatic data logging began in January 1988. Survey monuments were also placed in January 1988 and bimonthly surveys have been conducted since then by members of the US Geological Survey. Foundations for three seismometers were poured in March 1988 and the three instruments were installed in April. Members of Weidlinger Associates maintain and monitor the site approximately once a month. During these visits, the seismometer data tapes are replaced with blank tapes, and the contents of the data logger are examined.

Two major activities are planned for the upcoming year. First, to correlate the pipe strains and deformations with ground strains derived from the Japanese seismometers, it is necessary to upgrade the acquisition rate of the data logger. This is possible because commercial power is available at the site and can support the higher acquisition rate. This will be accomplished by acquiring and installing an upgrade package. Second, further efforts will be made to identify and eliminate sources of strain gage drift.

SECTION 2
CONSTRUCTION AND RECENT ENHANCEMENT OF INSTRUMENTATION

2.1 Previous Construction

The locations of the pipe segments at Owen's Pasture are shown in Figs. 2-1 and 2-2. One of the welded steel segments in Fig. 2-1 (marked T) is oriented at 40° counterclockwise with respect to the assumed strike of the rupture zone; it is designed to be subjected to combined tension and shear by right lateral strike slip. The other welded steel segment in Fig. 2-1 (marked C) is oriented at 40° clockwise with respect to the assumed strike of the rupture zone; it will be subjected to combined compression and shear by right lateral strike slip. Longitudinal measurements of strain are made with strain gages placed at the springline, or mid height of the pipe, on opposite sides of a diameter and hence are capable of measuring longitudinal strain and horizontal bending. These pipe segments are 12.75 inches outside diameter with 0.125 inch wall thickness. Yield stress of the pipe steel was measured between 41,000 psi and 48,000 psi; the steel exhibits considerable hardening, as is typical in many recently constructed pipelines. As shown in Fig. 2-1, the pipe is embedded in river sand with compacted native backfill above.

Eight 6-inch diameter ductile iron segments are also included as shown in Fig. 2-2. Four of these have unrestrained joints (TYTON, a trademark of US Pipe and Foundry Co.); they are oriented at 60° and 30° counterclockwise with respect to the strike of the rupture, and hence will be subjected to tension and shear. These segments are instrumented with displacement transducers designed to measure changes in length and rotation at the joint. The other four segments have restrained joints which are designed to prevent separation; they are not instrumented. These segments were laid in a two-foot wide trench excavated to a depth of four feet. The trenches were backfilled with river sand up to 3 to 6 inches above the crown of each segment. Native soil was replaced and compacted.

Both types of pipelines have concrete blocks formed around the ends to restrain their movement. The welded steel pipes require especially large restraining blocks due to the large longitudinal forces that can be generated by ground movement; based on preliminary estimates, each block is capable of resisting about 200,000 pounds force. The ductile iron pipes have much smaller anchors because the capacity of flexible joints for transmitting axial force is small.

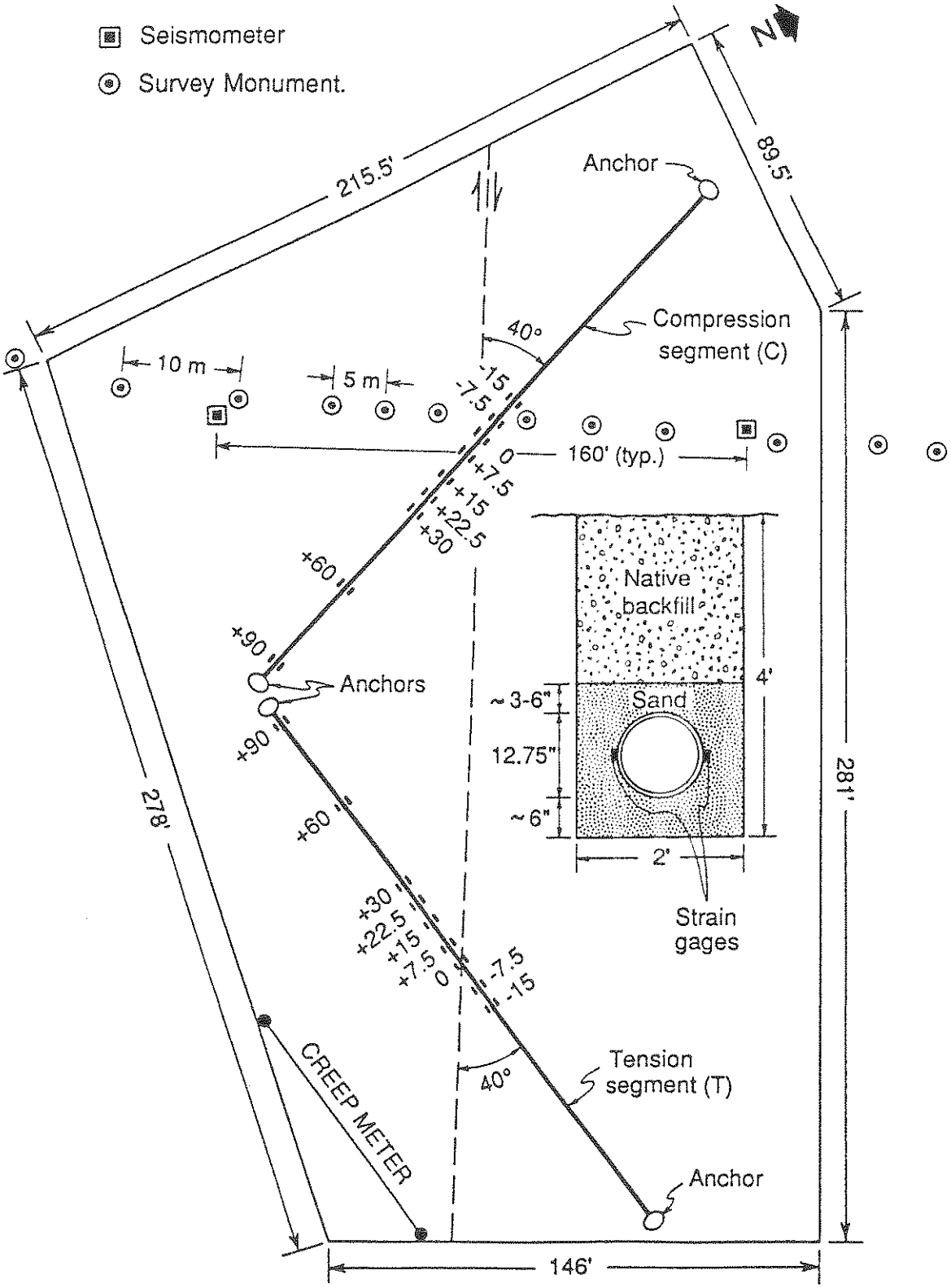

FIGURE 2-1 Orientation And Strain Gage Locations, Welded Steel Pipe Segments

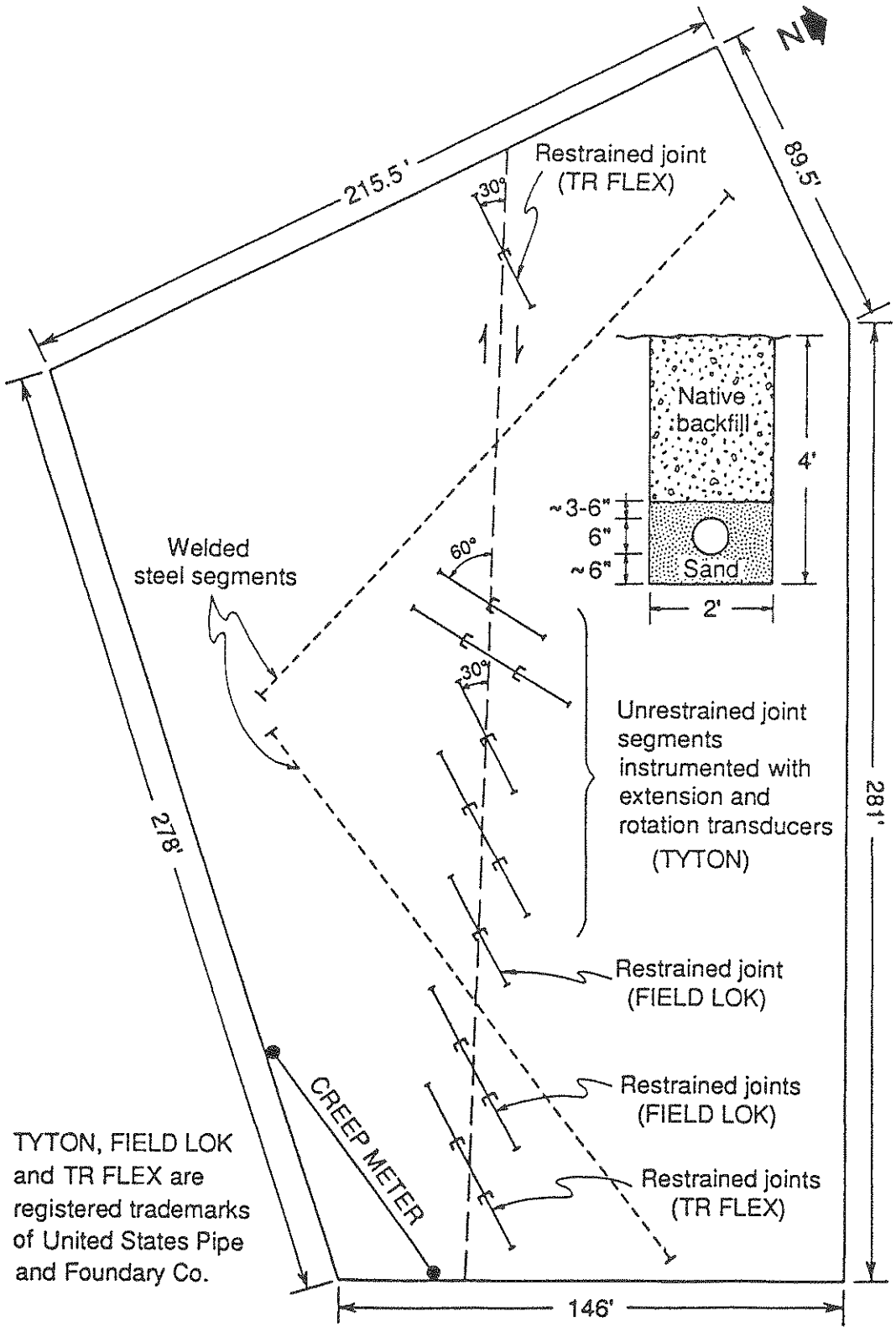

FIGURE 2-2 Orientation And Joint Types For Iron Pipe Segments

2.2 New Instrumentation

Two types of ground motion measurements are currently being made. An array of survey monuments was placed approximately on a straight line at nearly right angles to the assumed fault strike. As shown in Fig. 2-3, there are 12 such monuments with 5 meter spacing near the fault and 10 meter spacing at greater distances. The monuments were placed according to USGS practice in this area. First a 6 inch diameter post hole was dug 24 inches deep. Then a 1 inch diameter galvanized steel pipe 6 feet long was centered in the hole and then driven into the ground until the top of the pipe was just below the original ground surface. Finally, the hole was lined with PVC pipe, and a plug with a surveyors mark was fitted into the top of the pipe. An elevation view is shown in Fig. 2-4.

As of the date of this report, three surveys of this array have been made by USGS (Ref. 15); results are shown in Fig. 2-5. Displacements are reported for each survey relative to the positions of monuments in the reference survey. Stations are noted on the left margin and start at the top instrument station (IS01). Deflection (DS Stations), and End Station (ES01). Station distances are on the right margin and the scale is in the lower right corner. The following is an excerpt from Ref. 15:

> *The most significant movement occurred between monuments IS01 and DS03. Survey 3 represents approximately 6.6mm right-lateral displacement. Figure 2-3 is a site layout which includes the fault trace suggested by the trenches and observations prior to our array installation. The alignment array data thus far indicates the most active trace may be 10-30m to the southwest of the original estimate. It is important to note that four months' data is not enough to change original assumptions. However, the surveying techniques we use give a very conservative error bar of 2mm, which is significantly below our result of 6.6mm. In Fig. 2-5, apparently other faults exist elsewhere in the array. For example, in Survey 2, inflection points indicate possible traces at monuments DS05 and DS09. However, when comparing Surveys 2 and 3, no displacement is shown at these monuments.*

The second type of instrument is the three-axis seismometer which has been loaned to the project by the Urban Hazards Research Institute of the University of Kyoto. The locations of these three instruments are indicated in Fig. 2-1. The axes of horizontal response are aligned parallel and perpendicular to the assumed fault strike. Each instrument is mounted on a reinforced concrete pad with steel pipe pilings, as shown in Fig. 2-6. Specifications for the seismometers are given in

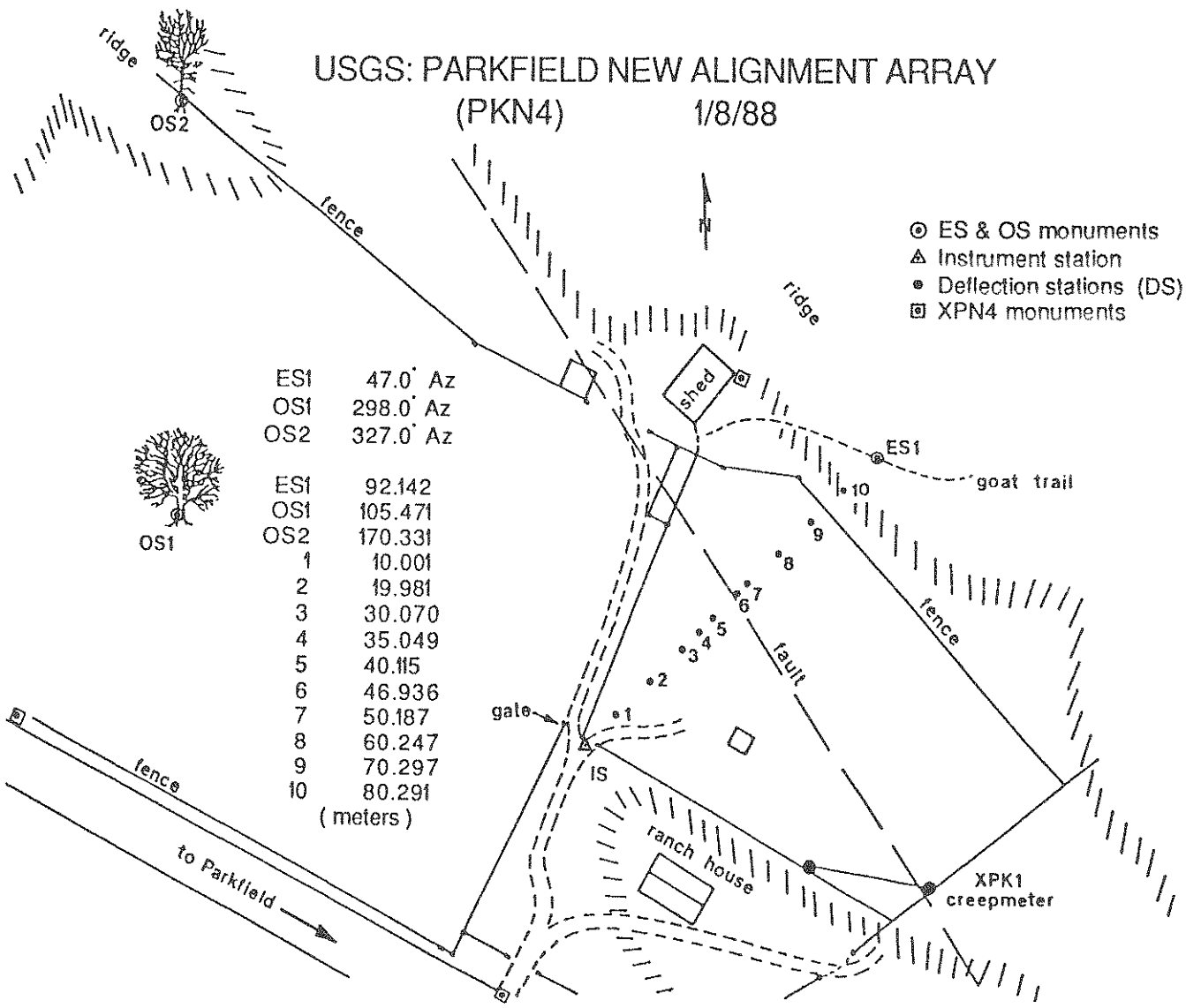

FIGURE 2-3 USGS Alignment Array (PKN4), Owens Pasture

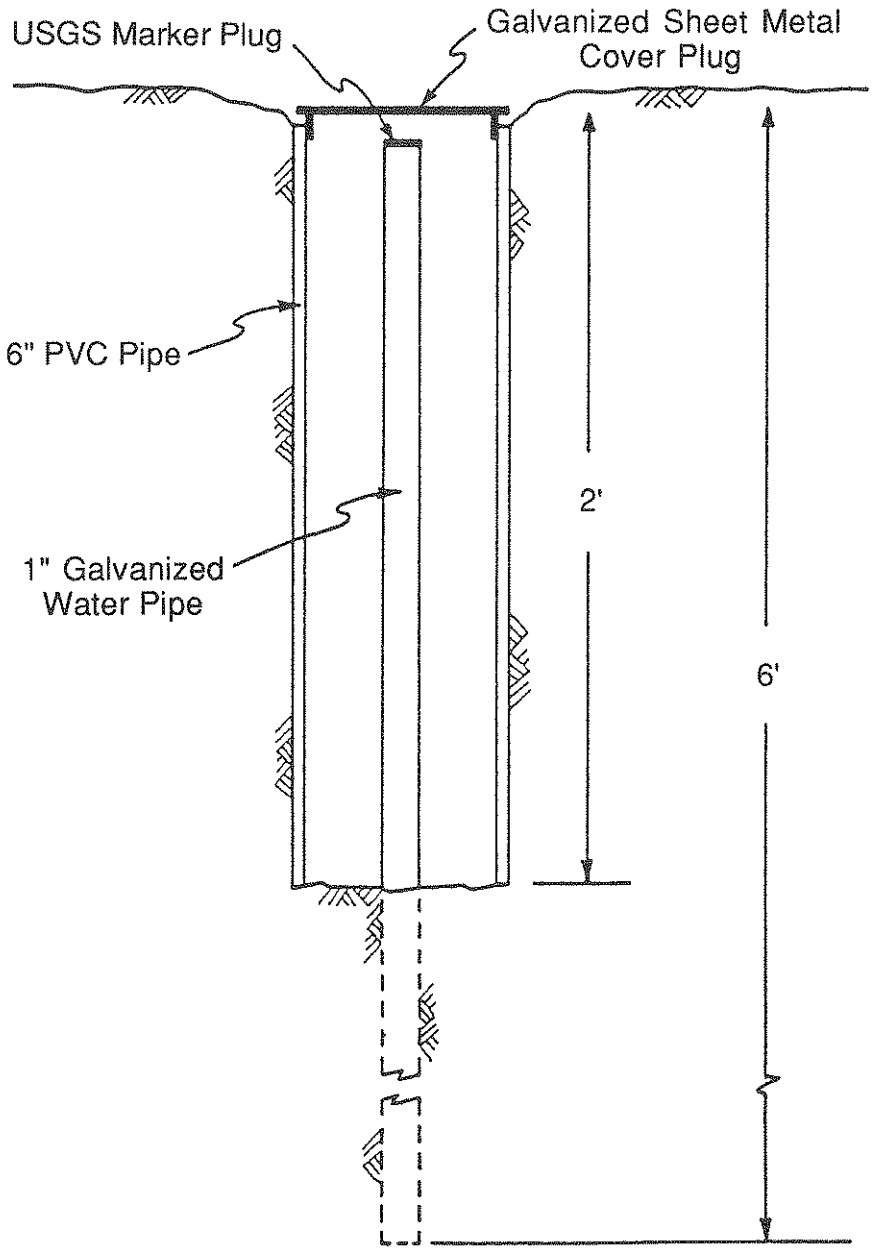

FIGURE 2-4 Survey Monuments

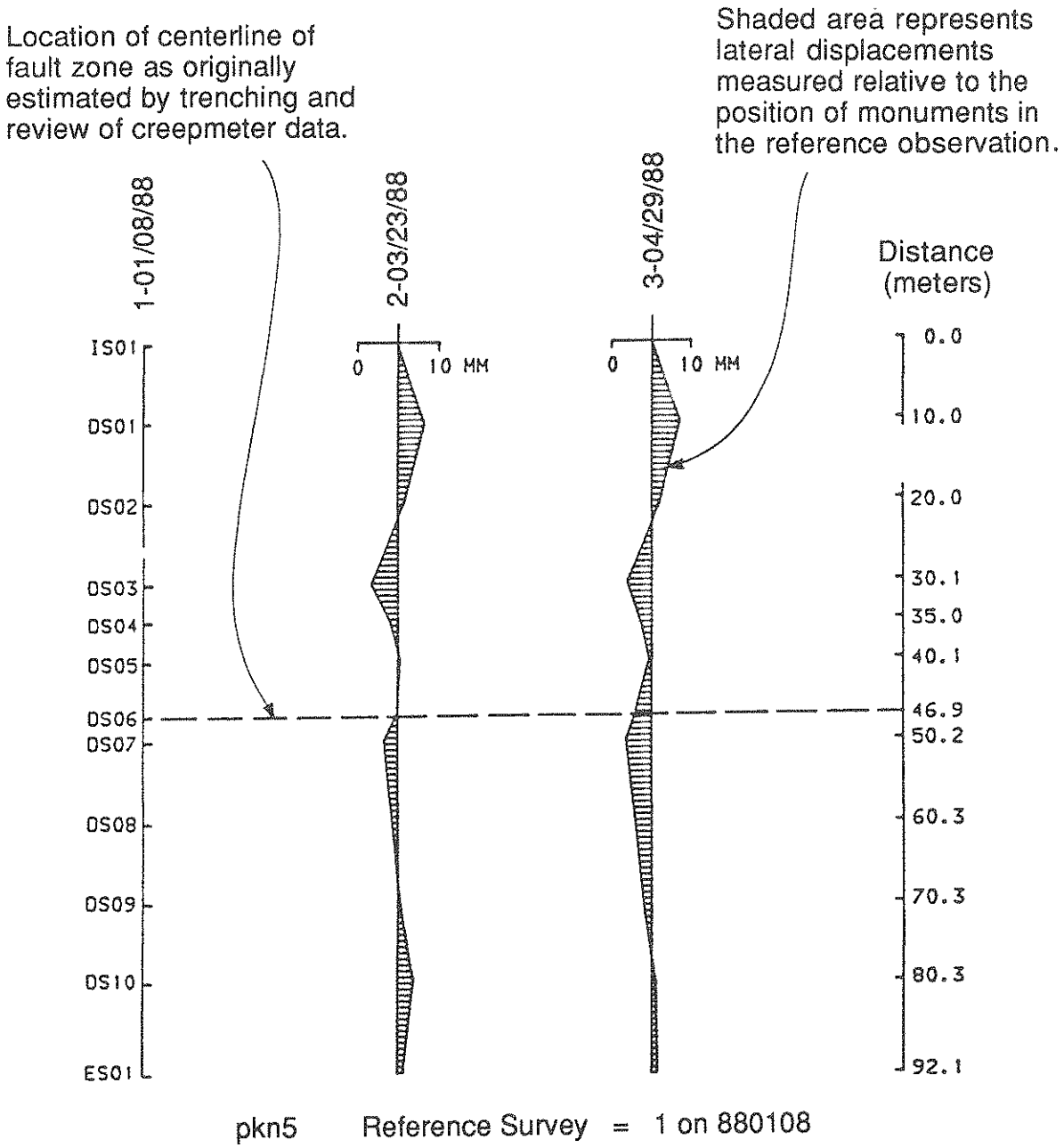

FIGURE 2-5 Creep Offsets Measured At Alignment Array On 3-23-88 And 4-29-88

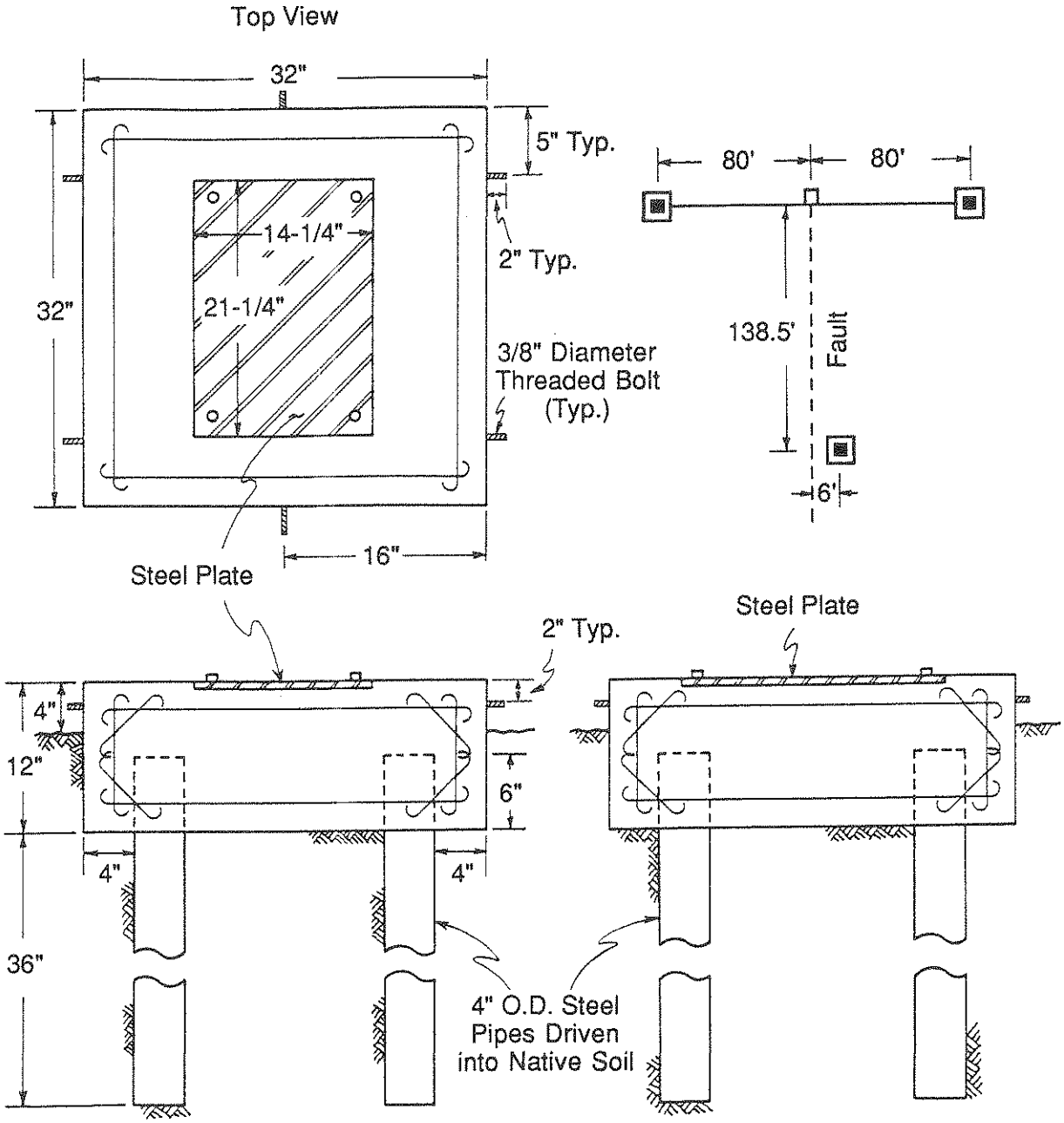

FIGURE 2-6 Details Of Seismometer Foundations

Appendix A. The purpose of the seismometers is not primarily to make point measurements of ground shaking, though of course they will do this. Instead, the primary purpose is to estimate ground strain from measurements of particle velocity , v(t), and phase velocity c. The approach to identifying wave types, directions and velocities adopted in Ref. 14 for interpreting SMART-1 strong motion data will be used in the present experiment. It is assumed in this analysis that the array of receivers is located at a laterally homogeneous site far enough from the source that the angle of incidence, predominant frequencies of phases and propagation velocities of the phases are approximately equal for all stations. This assumption will be satisfied for phases arriving at the Owen's Pasture array from a distant epicenter, such as occurred in 1966; it may not be satisfied for phases associated with ground rupture within a few feet of the array. Identifying a particular phase present in the ground motion requires that the motion be dominated by the particle motion of a single phase at a specific frequency. For the example shown in Appendix B, the distance from the epicenter to an array of receivers with a 4 km aperture is on the order of 30 km, which produces response that allows several phases to be identified and gives approximately equal dominant directions of motion at all stations for the phases. The expression

$$\varepsilon(t) = \frac{v(t)}{c} \tag{2-1}$$

will be evaluated. The quantity $\varepsilon(t)$ will be resolved into directions parallel and perpendicular to the pipe axes and then related to the strain in the steel pipe segments and to the displacements and rotations of joints in the ductile iron segments.

SECTION 3
PROPERTIES OF STEEL PIPE AND PIPE-SOIL INTERFACE

3.1 Stress-Strain Characteristics Of Pipeline Steel

Three direct tensile tests were performed, Ref. 17, according to ASTM E8-85b, Ref. 16, on specimens of steel from the test pipe. Tensile coupons were cut from locations along the pipe circumference as indicated in Fig. 3-1. Test Specimen No. 3 was taken from a location adjacent to the longitudinal welded seam of the pipe. Test Specimens Nos. 1 and 2 were taken from locations approximately one-quarter of the circumference from the longitudinal seam, as shown in the figure.

All specimens were instrumented with three bondable strain gages as illustrated by Fig. 3-2, in which the approximate dimensions of the test specimens are shown. The strain gage used was Model CEA-06-250UW, manufactured by Micro Measurements Division, Raleigh, NC. An extensometer, Model EZ2-1, manufactured by United Calibration, Garden Grove, CA, was employed with Specimen Nos. 1 and 2 to measure the extension of an initial 1-inch-long section at the middle of the specimen. Strains were evaluated from the extensometer data by dividing the elongations by the initial 1-inch section length. In addition, the distance along each specimen between the upper and lower loading clamps was measured initially and after failure by carefully piecing together the broken portions. The difference in these lengths divided by the initial length was used to estimate the strain at rupture.

A Model 507A90649 hydraulic testing machine, manufactured by Wiedman Balchrin, King of Prussia, PA, was used to load the specimens. Special moment reducing clamps were employed to hold the specimens. All measurements were recorded by an automatic data acquisition system, Model HP 33052A, manufactured by Hewlett Packard, Palo Alto, CA.

Figures 3-3 through 3-4 show tensile strain as a function of tensile stress for Specimen Nos. 1, 2 and 3, respectively. All strains are plotted in terms of microstrain, a single value of which is 1×10^{-6}. In Figs. 3-3 and 3-4, strains are plotted as measured by both the strain gages and the extensometer. There was very good agreement between the two methods of measurement. The break point strain indicated by the (+) sign, in Figs. 3-3 to 3-5, was determined by piecing together broken portions of the specimen and measuring changes in length relative to the initial length.

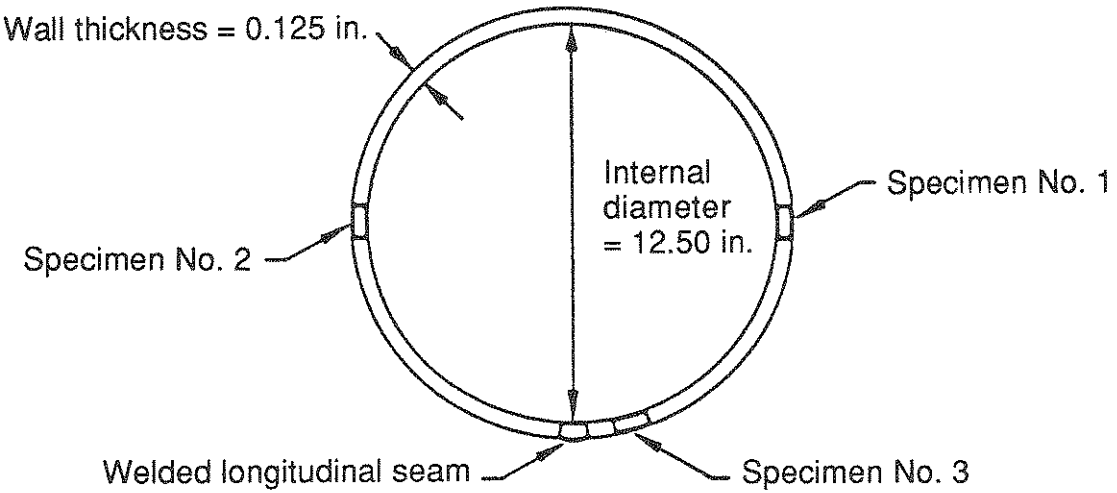

FIGURE 3-1 Pipe Cross-Section Showing Locations Of Steel Test Specimens

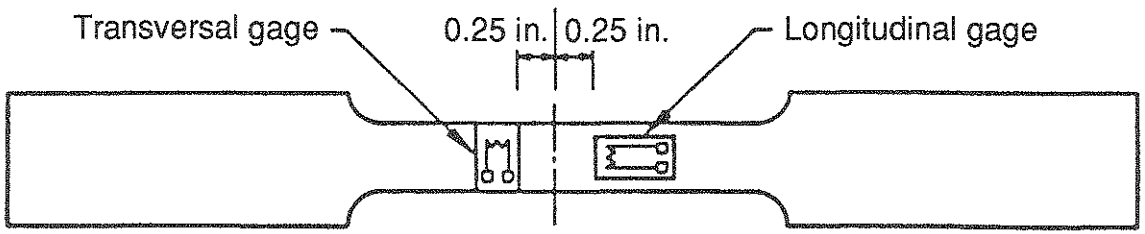

a) Front View

Specimen thickness
= 0.100 to 0.125 in.

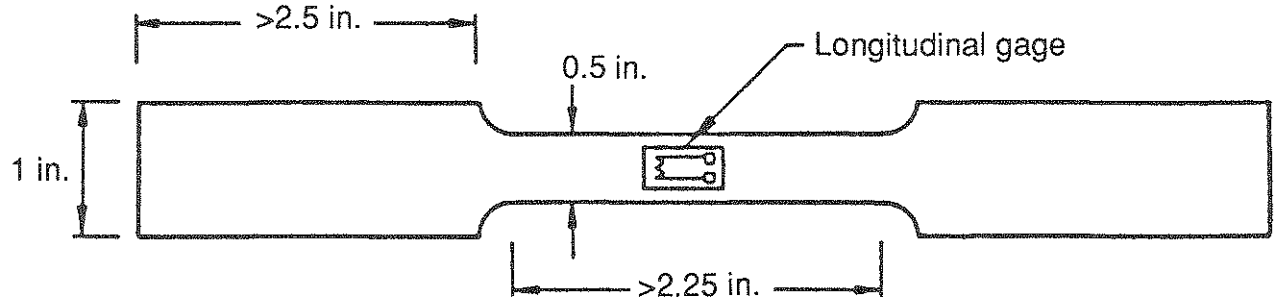

b) Rear View

FIGURE 3-2 Front And Rear Views Of Tensile Specimens

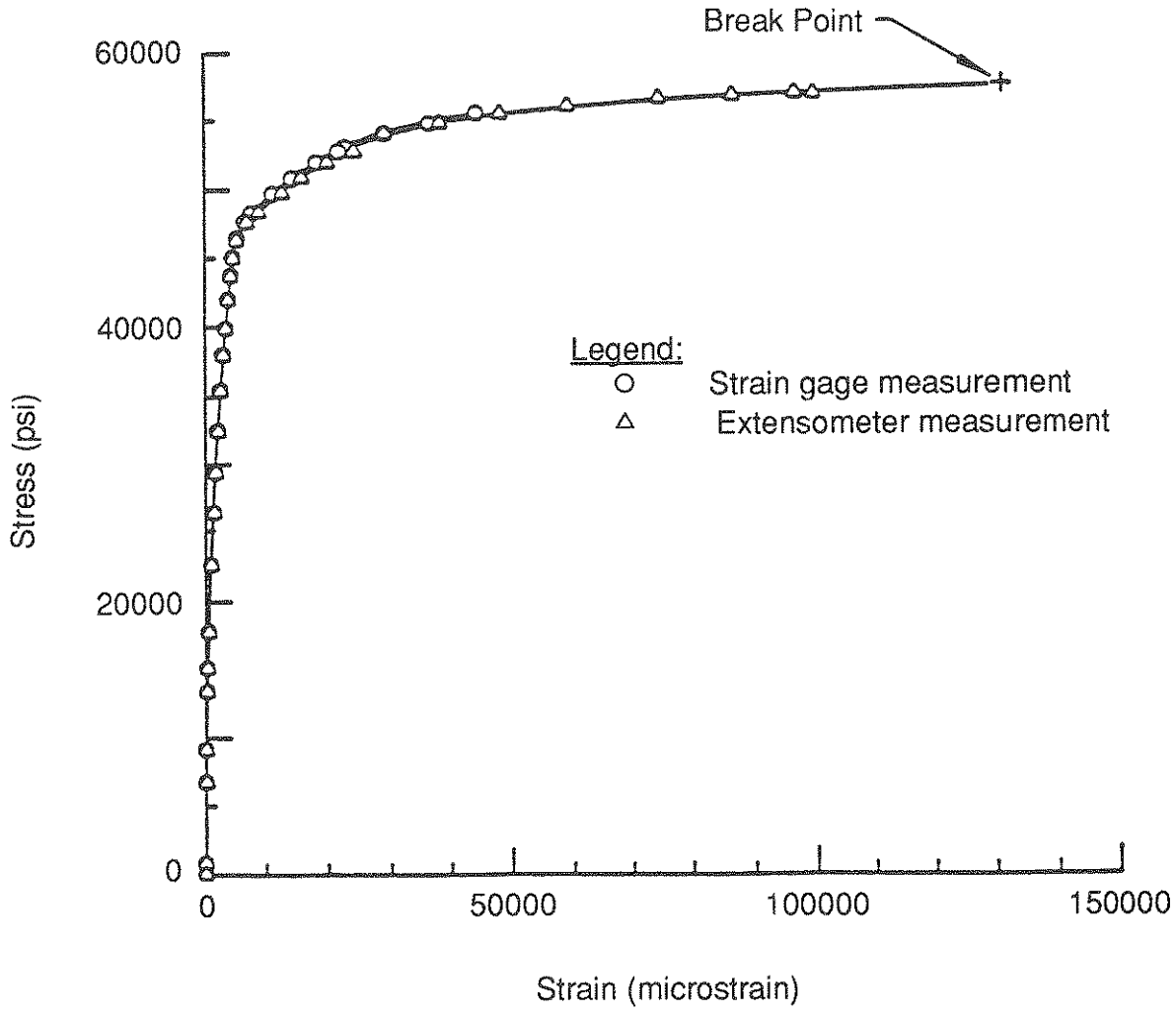

FIGURE 3-3 Tensile Stress Versus Strain For Test Specimen No. 1

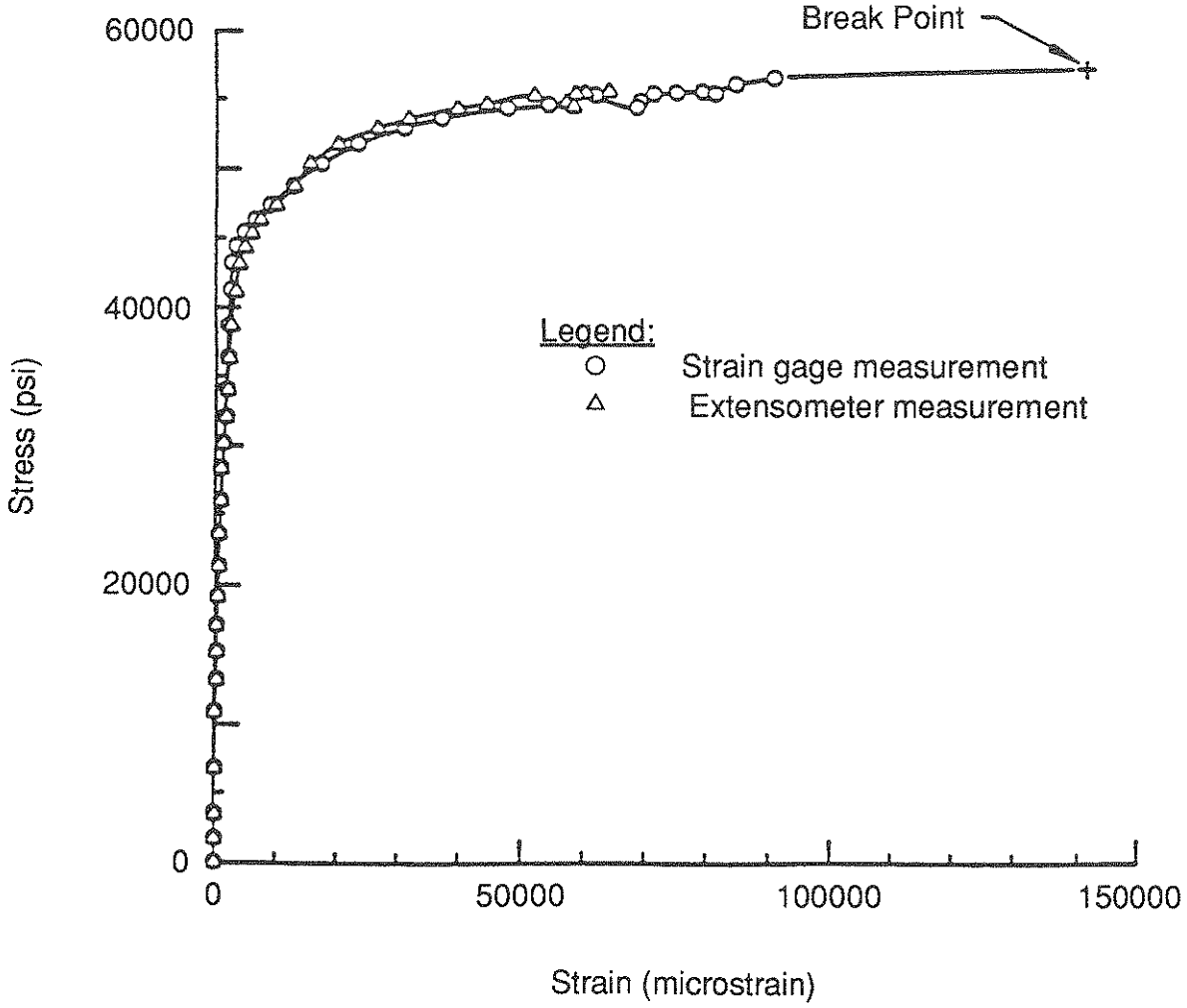

FIGURE 3-4 Tensile Stress Versus Strain For Test Specimen No. 2

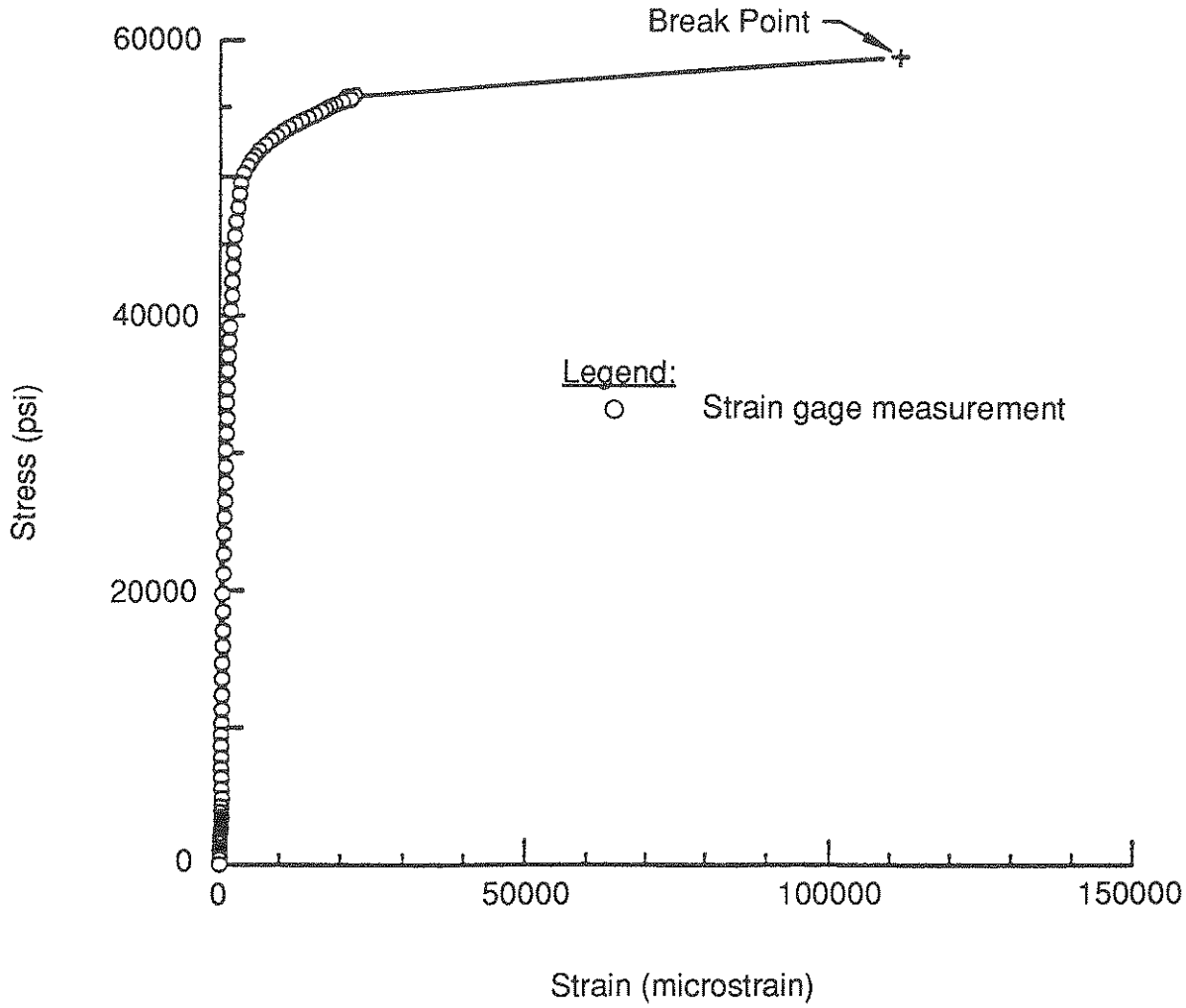

FIGURE 3-5 Tensile Stress Versus Strain For Test Specimen No. 3

Table III-1 summarizes the yield and ultimate stresses pertaining to each test specimen. All specimens failed at an ultimate stress of approximately 57,000 to 58,000 psi at strains ranging from 11 to 14.5%. The yield stress was evaluated by means of the offset method, Ref. 16, by taking an offset of 0.2% and assuming the proportional limit at 30,000 psi. The yield stresses from Specimen Nos. 1 and 2 are very close, whereas the yield stress for Specimen No. 3 is approximately 6,000 psi higher at 48,000 psi.

Figures 3-6 and 3-7 represent trilinear and Ramberg-Osgood representations, respectively, of the stress-strain relationship for Specimen No. 3. The Ramberg-Osgood formulation (Ref. 4) to represent the nonlinear stress-strain behavior of steel may be expressed as

$$\varepsilon_a = \frac{\sigma}{E_1}\left[1 + \frac{\alpha}{(r+1)}\left(\frac{\sigma}{\sigma_E}\right)^r\right] \tag{3-1}$$

in which σ and ε_a axial stress and strain, respectively E_1 is Young's modulus, α and r are Ramberg-Osgood coefficients, and σ_E is the effective yield stress of the steel.

3.2 Soil-Pipe Interface Shear Characteristics

Direct shear tests were performed to measure the shear characteristics at the interface between the test pipe steel and sand backfill. The tests were conducted with a direct shear box manufactured by Wyckham-Farrance, Ltd., London, UK, which provides a shear contact surface of 2.45 x 2.45 inches between the upper and lower parts of the device. The interface strength characteristics for sands and various metals and concrete surfaces have been published and widely disseminated on the basis of tests conducted with this type of equipment, Refs. 18 and 19.

Sections of steel were cut from the test pipe wall and flattened by means of a roller press. The steel specimen, approximately 0.125 inch thick, was fixed to a rigid plywood base and positioned in the bottom half of the direct shear apparatus, such that the steel surface was 0.002 inches above the horizontal plane of the bottom box. Air-dried specimens of sand were poured carefully onto the steel surfaces from a height of 2 inches above the top of the sand until the upper part of the direct shear box was filled. This method of placement resulted in dry unit weights ranging from approximately 97 to 104 pcf. Increased unit weight was achieved by densifying the soil with a sanding vibrator. The unit weight was determined by dividing the weight of the sand

TABLE III-1 Summary Of Yield And Ultimate Stress For Test Pipe Steel

Specimen Number	Yield Stress, psi[a]	Ultimate Stress, psi
1	42,000	57,000
2	41,000	57,000
3	48,000	58,000

[a] Determined at 0.2% offset corresponding to 30,000 psi proportional limit; see Ref. 16.

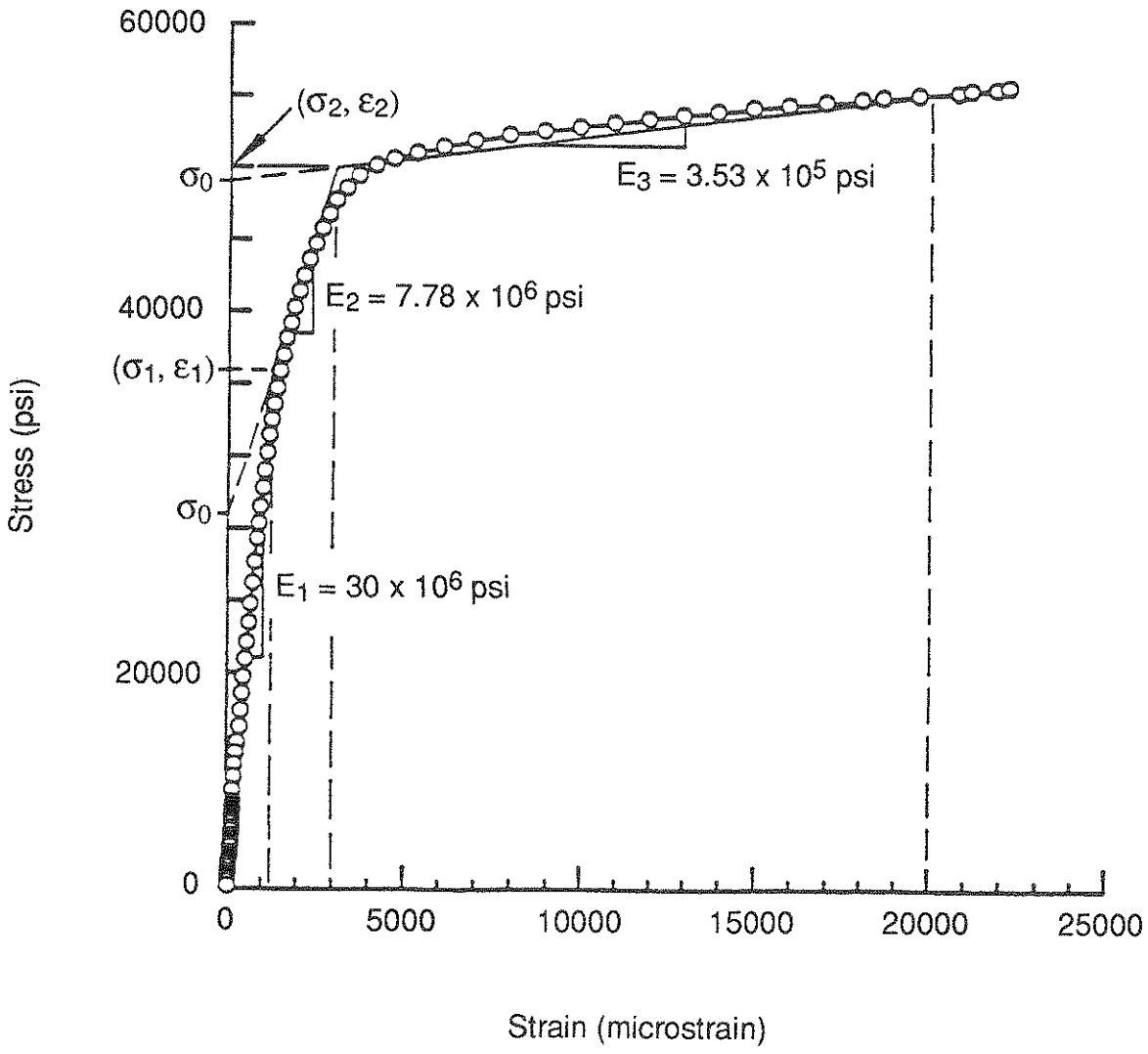

FIGURE 3-6 Trilinear Representation Of Stress-Strain Plot Of Specimen No. 3

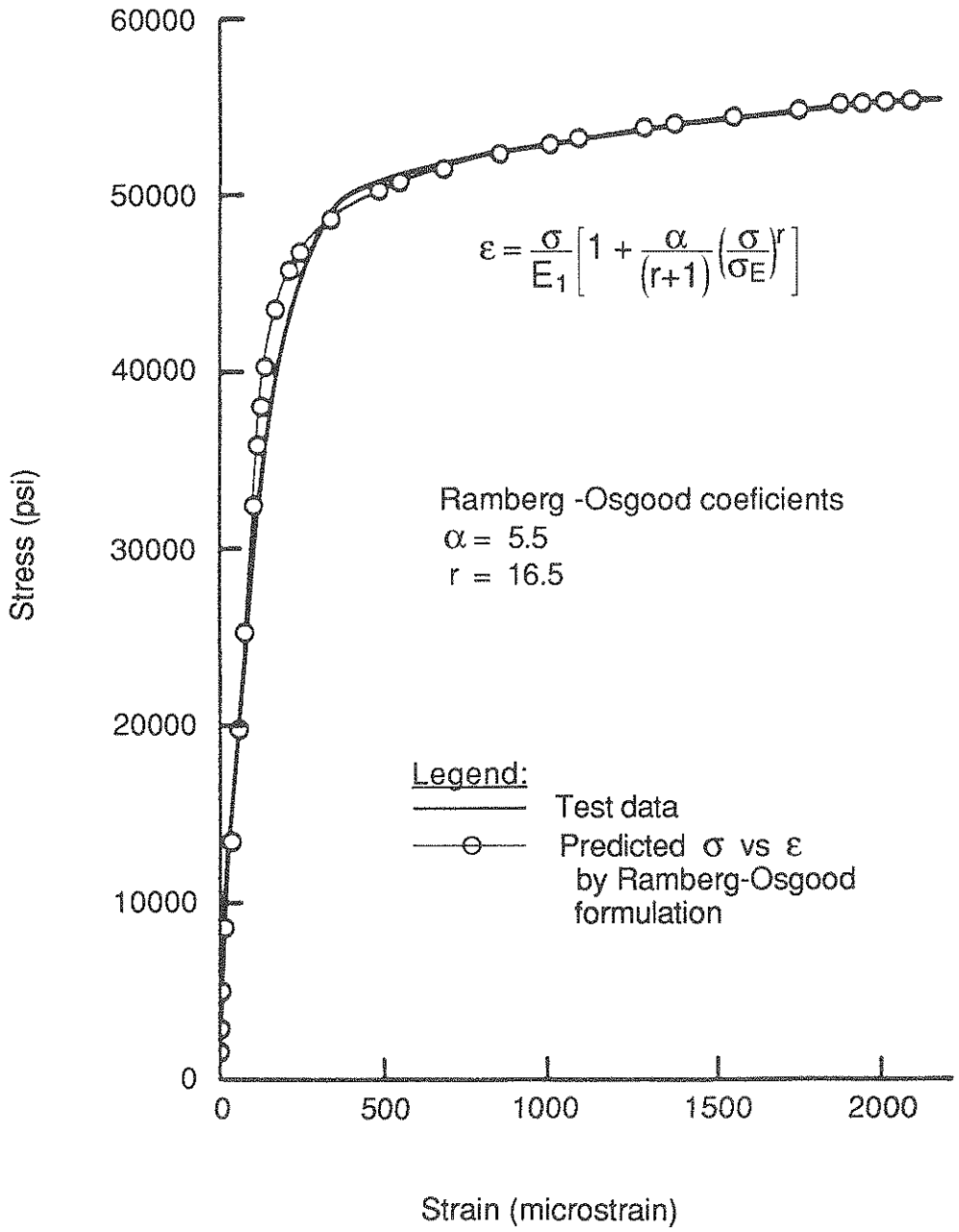

FIGURE 3-7 Ramberg-Osgood Representation Of Stress-Strain Plot Of Specimen No. 3

by the volume it occupied in the apparatus. Volume measurements were accurate to within ± 0.5%.

The relatively small size of the direct shear box allowed for rapid and relatively easy sample preparation so that several variables could be studied. A total of 27 direct shear tests were performed to ascertain the strength properties of the sand and sand-steel interface for different unit weights of the sand. The rate of shear displacement varied from 0.01 to 0.02 inches/minute. For each test approximately 30 horizontal and vertical displacement measurements were obtained by means of a direct current differential transformer with a sensitivity of 0.0002 inches. Shear stress measurements were acquired through an electronically instrumented proving ring with a sensitivity of 0.01 psi. Normal stresses were established by means of dead load application to within 0.01 psi. All tests were run with a separation of 0.016 inches between the upper and lower portions of the direct shear apparatus.

A special upper frame of the shear box, composed of maplewood, was used for the testing. This frame weighed 0.24 lbs., compared with the 2.84 lb. brass frame provided by the manufacturer. Minimizing the weight of the upper frame was important for an accurate evaluation of normal stress in the relatively low range (3 to 10 psi) required to duplicate stress conditions for shallow pipe burial.

The sand used in the direct shear tests was the same material used as backfill immediately surrounding the test pipelines. It is a coarse to medium sized sand, which is subangular to angular in shape. The material is composed of quartz, feldspars, and various ferro-magnesium particles. The grain size distribution plot for the sand is shown in Fig. 3-8.

Figure 3-9 shows typical direct shear data for Test Nos. 1 and 5 on sand-steel interfaces. Both the shear stress and vertical loading cap displacement are plotted as a function of the horizontal displacement. The test data were obtained for dry unit weights 101.6 pcf (Test No. 1) and 109.6 pcf (Test No. 5) and a normal stress of 3 psi, which is consistent with the stresses at the burial depth of the test pipelines. The vertical displacements for sand with a dry weight of 101.6 pcf are very small, indicating virtually no volume change. In contrast, the vertical displacements for sand with a dry weight of 109.6 pcf are significant and indicative of dilative behavior. There is a peak shear stress for Test No. 5 at about 0.04 inches of horizontal displacement, after which the shear stress decreases to a steady state value consistent with the maximum stress measured in Test No. 1. Dilatancy and strain softening behavior was observed for tests of sand-steel interfaces when the sand unit weight was greater than about 107 pcf.

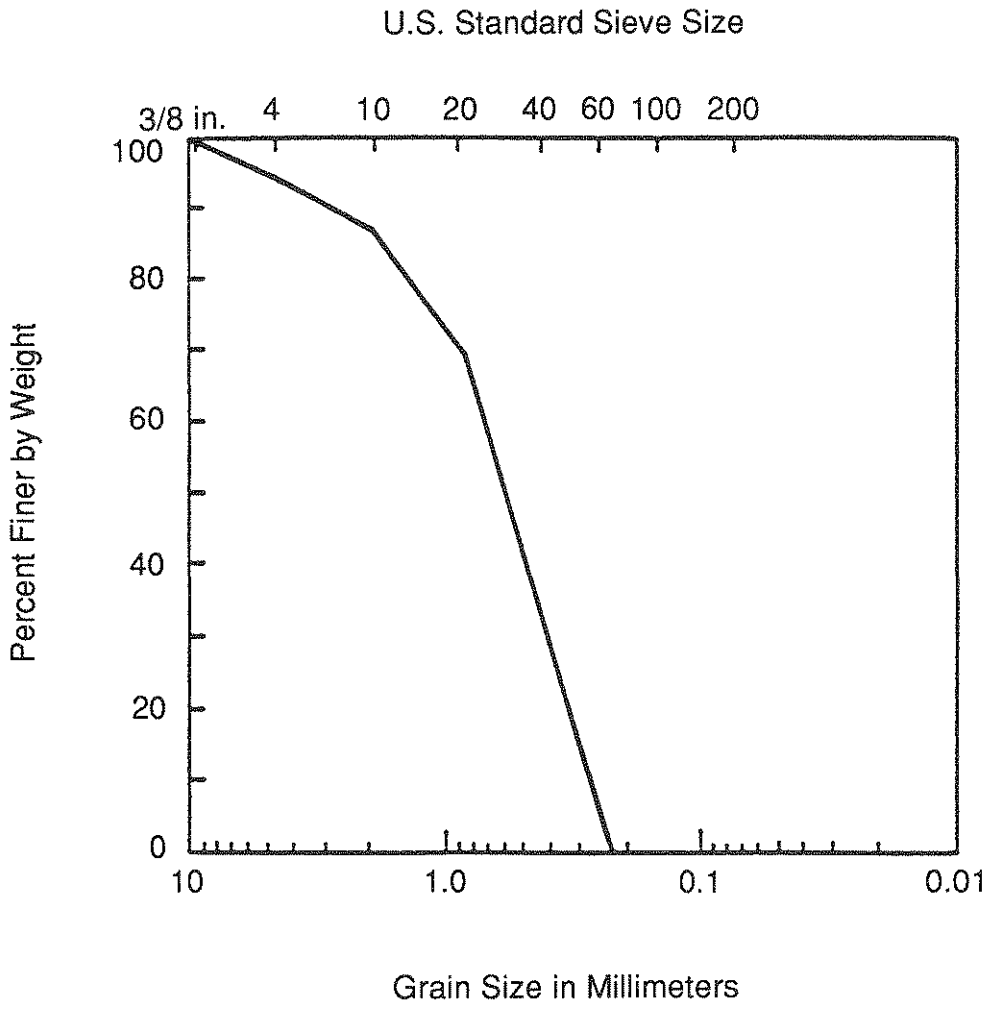

FIGURE 3-8 Grain Size Distribution Of Sand Backfill

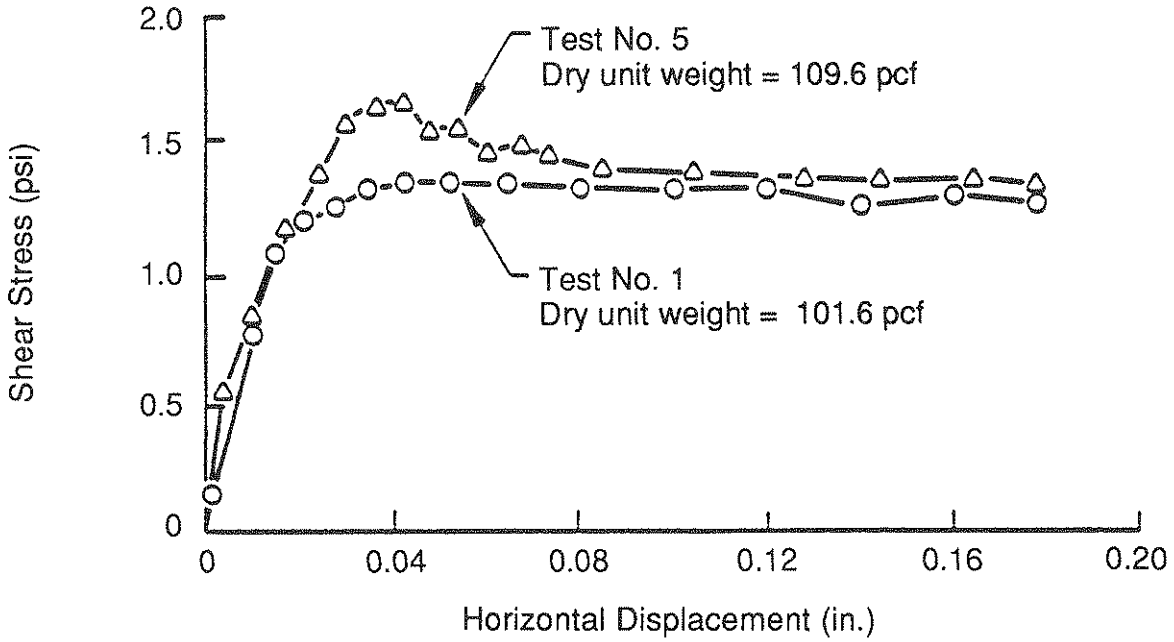

a) Shear Stress vs. Horizontal Displacement

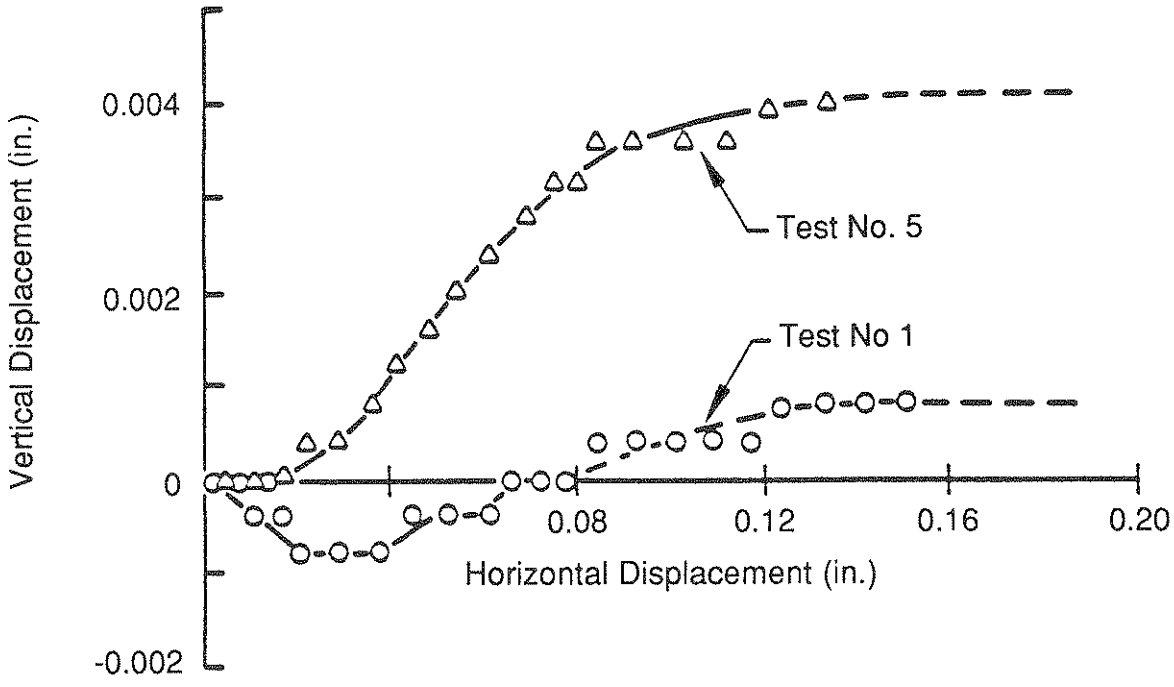

b) Vertical vs. Horizontal Displacement

FIGURE 3-9 Typical Direct Shear Test Results For Sand-Steel Interfaces At A Normal Stress Of 3 Psi

Table III-2 summarizes the test data. Each test is numbered from 1 to 27. The unit weight of sand at the beginning of each test is listed as well as the normal stress and maximum shear stress measured during the test. Peak angles of shear resistance, ϕ', and of the interface shear resistance between sand and steel, δ, also are listed.

Figure 3-10 shows the peak shear stress plotted as a function of the normal stress for the sand and sand-steel interfaces. The data pertain to dry unit weights of approximately 97 to 103 pcf, which range from a low to a medium dense sand, respectively. The angles of shear resistance of the sand, ϕ', and sand-steel interface, δ, are 38° and 26°, respectively. These values correspond to δ/ϕ' of approximately two-thirds, which agrees well with the results of previous studies, Ref. 18.

Figure 3-11 shows the peak angles of shear resistance for both the sand and sand-steel interfaces plotted as a function of the dry unit weight of the sand. The best straight line fits, determined by linear regression analyses, are shown in the figure. Coefficients of correlation for each of the linear plots also are indicated. There appears to be a good linear correlation between the maximum friction angle and dry unit weight of the sand. It should be recognized that the rate at which the friction angle for the sand-steel interface increases, relative to sand unit weight, is low. The range of δ for all unit weights tested is only 22.8° to 28.6°.

3.3 Summary

Direct tension tests on three specimens of steel from the test pipeline show ultimate stresses at rupture of 57,000 to 58,000 psi at tensile strains of approximately 11.0 to 14.5%. The yield stress of the steel adjacent to the longitudinal seam of the pipe is approximately 48,000 psi. The yield stresses evaluated from specimens one-quarter of the circumference from the seam are 41,000 and 42,000 psi. Trilinear representations have been developed in this report for the tensile stress-strain relationships pertaining to steel specimens with maximum and minimum yield stresses.

Direct shear tests of the sand backfill and sand-pipe steel interface show the angles of shear resistance for both conditions increase linearly as a function of sand unit weight. Variations of the interface friction angle, δ, however, are small when correlated with unit weight, and a relatively narrow range of $23° \leq \delta \leq 28°$ appears to cover virtually all circumstances, provided that significant rusting or pitting of the pipe surface does not occur. Peak, or maximum, shear resistance along the sand-pipe interface is mobilized at about 0.04 inches of relative movement.

TABLE III-2 Summary Of Peak Measurements For Direct Shear Tests Of Sand And Sand-Steel Interfaces.

Test No.	Dry Unit Weight lbs/ft^3	Normal Stress, psi	Peak Shear Stress, psi	Sand-Steel Interface Friction Angle, δ, degrees	Angles of Shear Resistance of Sand, ϕ', degrees
1	101.6	3.00	1.38	24.7	
2	101.0	3.00	1.36	24.4	
3	107.6	3.00	1.50	26.7	
4	107.8	3.00	1.46	25.9	
5	109.6	3.00	1.63	28.6	
6	98.7	3.00	1.32	23.7	
7	97.3	3.00	1.33	24.0	
8	96.9	5.00	2.10	22.8	
9	101.1	5.00	2.39	25.6	
10	101.2	5.00	2.33	25.0	
11	100.6	5.00	2.18	23.6	
12	102.9	10.00	4.74	25.4	
13	102.1	10.00	4.89	26.1	
14	102.3	10.00	5.02	26.7	
15	99.8	10.00	8.08		39.0
16	97.2	10.00	7.08		35.3
17	96.1	10.00	8.01		38.7
18	96.2	5.00	3.45		34.6
19	96.8	5.00	3.77		37.1
20	96.1	5.00	3.50		35.0
21	94.3	3.00	2.00		33.7
22	95.1	3.00	1.97		33.3
23	100.0	3.00	2.43		39.1
24	100.1	3.00	2.55		40.4
25	103.8	3.00	2.82		43.2
26	105.0	3.00	3.01		45.2
27	107.0	3.00	3.44		49.0

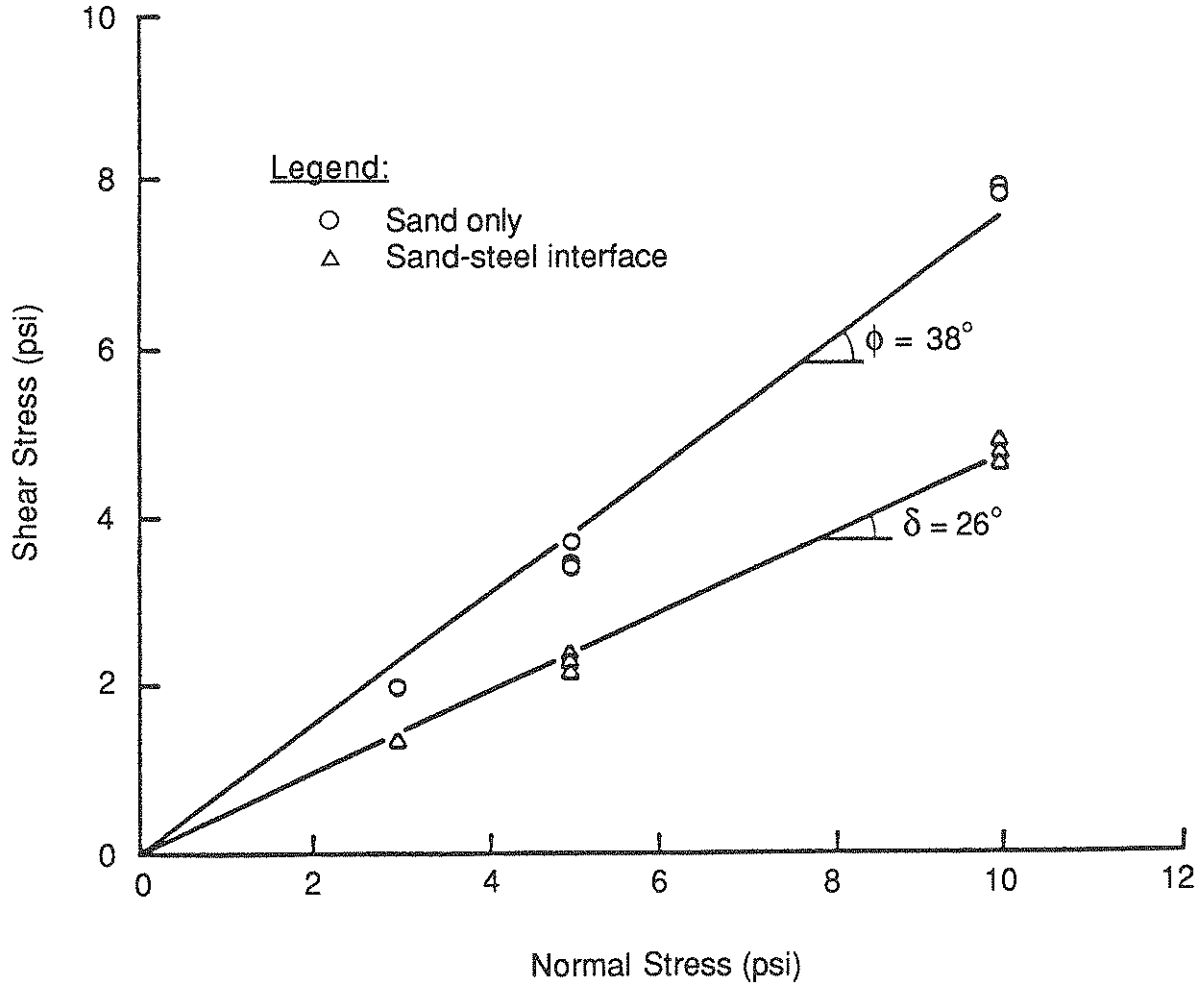

FIGURE 3-10 Peak Shear Stress As A Function Of Normal Stress For Sand And Sand-Steel Interfaces

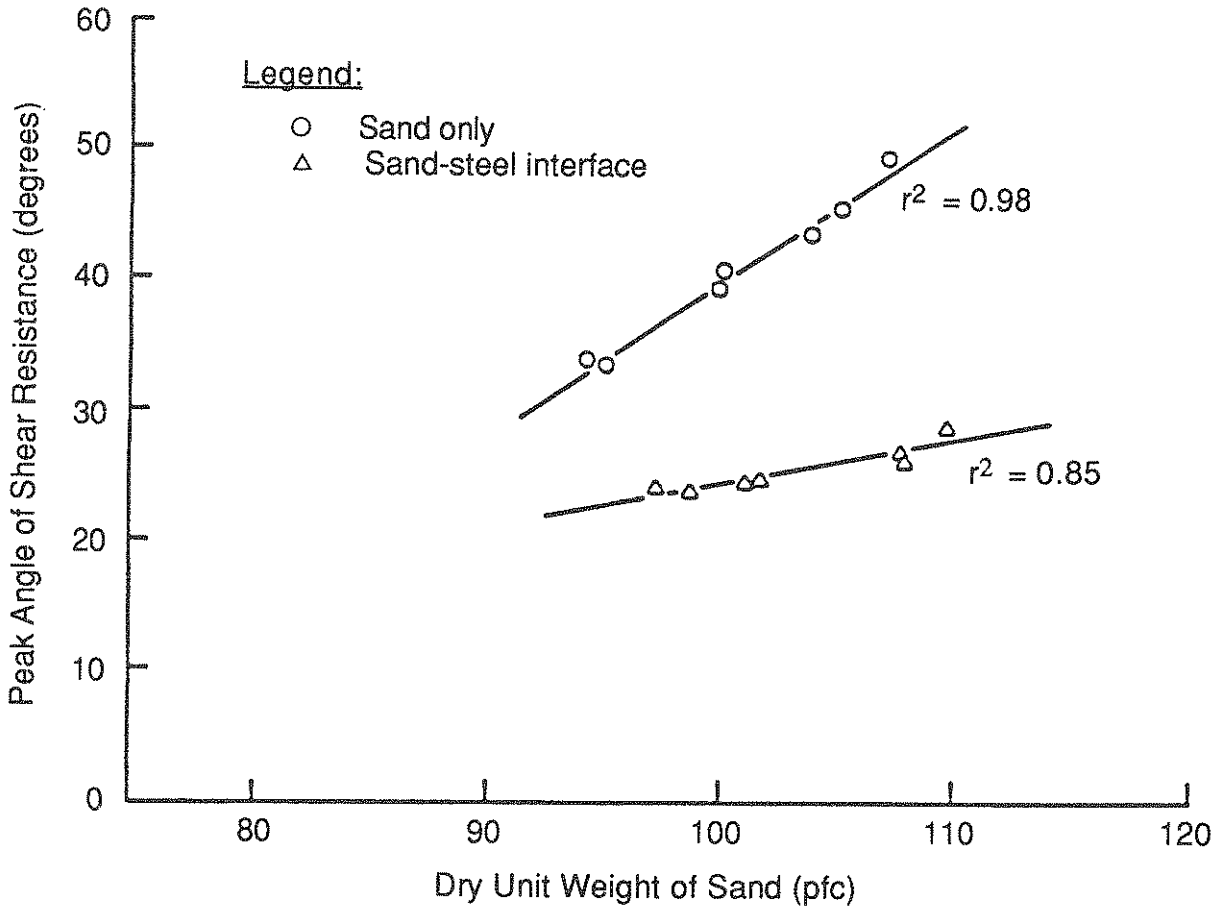

FIGURE 3-11 Angles Of Shear Resistance For Sand And Sand-Steel Interfaces As A Function Of Dry Unit Weight

SECTION 4
PREDICTED RESPONSE

4.1 Analytical Model Predictions

Given the test data pertaining to the steel and shear characteristics of the sand-steel interface, it is possible to evaluate the maximum strain in the test pipeline for a right lateral strike-slip movement of four inches along the San Andreas Fault. Calculations based on the Newmark, Hall and Kennedy, et al. models (Refs. 3 and 4) of pipeline response to fault movement are given in Appendices B and C.

It is assumed that the test pipeline is buried at a depth of 3 feet from ground surface to top of pipe. If the sand backfill was placed to be medium dense with a dry unit weight of 105 pcf, then reference to Fig. 3-11 indicates that the interface friction angle, δ, is 25°. Based on the assumption that the sand is partially saturated, the unit weight of the backfill in situ is estimated to be 115 pcf. The stress-strain properties of the steel are modeled by means of the Ramberg-Osgood representation shown in Fig. 3-7, which is used in the calculations involving the Kennedy, et al. model.

Application of the Newmark-Hall model for the aforementioned assumptions gives a maximum tensile strain in the pipeline marked T in Fig. 2-1 of 0.18% at the fault crossing. Application of the Kennedy, et al. model gives a maximum axial strain of 0.16% at the fault crossing, and also results in a maximum bending strain of approximately 0.70%. Hence, the maximum combined strain from summing the axial and bending components is 0.86%, which substantially exceeds the 0.18% strain predicted by the Newmark-Hall model.

Use of the Kennedy, et al. model for this situation is not strictly consistent with the model assumptions. Kennedy, et al. assume that the pipeline behaves as a cable, i.e., that lateral forces from the soil are supported by axial tension, acting through the longitudinal curvature of the pipeline, rather than by developing bending moment. For the fault displacement expected at Owen's Pasture, the pipeline will support soil loads by means of both bending and axial stiffness. Accordingly, the Kennedy, et al. analysis is likely to overestimate strain because it overestimates curvature by neglecting the bending stiffness of the pipeline.

The experiment at Parkfield is designed for conditions of deformation that are not fully addressed in either the Newmark-Hall or Kennedy, et al. models. Of significant interest is the bending strain generated by small to moderate fault offset, the zone in which pipeline bending occurs, and the influence of this flexural distortion on the accumulation of axial elongation as progressively larger amounts of fault offset occur. The experimental pipeline at Owen's Pasture will help clarify the first two of these issues, and will provide indirect evidence of the latter.

Both the Newmark-Hall and Kennedy, et al. models superimpose a constant curvature at the inflection point of the pipeline. This is physically impossible because an inflection point, by definition, cannot be subject to curvature. Under real conditions, the maximum curvature and axial elongation will not occur at the same location. The experimental pipeline at Parkfield will help to clarify this condition by providing data on how axial and bending strains are actually distributed relative to the fault crossing.

4.2 Computation Of Phase Velocity

Following Penzien and Loh, Ref. 14, the Fourier transform of a ground motion using time and frequency domain windows centered on t_o and f_o are given by Eqs. (4-1) and (4-2). In the initial step in the analysis, a Fourier transform is performed on the ground motion in the x and y directions for a specific frequency, f_o, using a time window that includes all significant high intensity portions of the time history. The variance function for a pair of time histories, x_i and x_j, and a time lag, τ, is defined by Eq. (4-3). The ground motion in the x and y directions can be resolved along axes x' and y', which are rotated by an angle ϕ, by Eq. (4-4). The direction of maximum intensity of the ground motion at a frequency f_o can be obtained by maximizing the variance function, $R_{x'x'}$ (t=0), with respect to ϕ. This term is called the principal variance. The angle ϕ_o, in Eq. (4-5), defines two principal directions, x" and y", 90° apart. The principal variances along the principal directions are given by $R_{x"x"}$ (f_o) and $R_{y"y"}$ (f_o). A principal variance ratio $R(f_o)$ is defined by Eq. (4-6). $R(f_o)$ varies over a range $0 < R < 1$. When $R(f_o)$ equals 1, the motions consist of two equal amplitude harmonics traveling in orthogonal directions 90° out of phase. If $R(f_o)$ equals 0, the motion is a single harmonic traveling in a straight line. The analysis outlined above is performed over a range of frequencies and the principal variance, principal variance ratio and f_o are plotted as a function of frequency. For determining the different phases present in a ground motion, attention is given to frequencies where $R(f_o)$ approaches zero, since this signifies that the motion of a single phase dominates the response at that frequency.

Fourier amplitude of ground motion, x(t) component centered on t_o is $A_x(f)$.

$$A_x(f) = \int_{t_o - \frac{\Delta t}{2}}^{t_o + \frac{\Delta t}{2}} x(t) \exp(-i2\pi ft)\, dt \tag{4-1}$$

Recovered ground motion component x(t) centered on time and frequency windows t_o and f_o, respectively.

$$x(t) = \int_{-f_o - \frac{\Delta f}{2}}^{-f_o + \frac{\Delta f}{2}} A_x(f) \exp(i2\pi ft)\, df + \int_{f_o - \frac{\Delta f}{2}}^{f_o + \frac{\Delta f}{2}} A_x(f) \exp(i2\pi ft)\, df \tag{4-2}$$

The variance function for two time-histories $x_i(t)$, $x_j(t)$ centered as in Eq. 3 is

$$R_{x_i x_j}(\tau) = \int_{t_o - \frac{\Delta t}{2}}^{t_o + \frac{\Delta t}{2}} x_i(t)\, x_j(t+\tau)\, dt \tag{4-3}$$

The resolved components of x(t), y(t) rotated through an angle ϕ are as follows:

$$\begin{aligned} x'(t) &= x(t)\cos\phi + y(t)\sin\phi \\ y'(t) &= -x(t)\sin\phi + y(t)\cos\phi \end{aligned} \tag{4-4}$$

The direction ϕ_o at which intensity of ground motion at a frequency f is maximum is

$$\phi_o(f) = \frac{1}{2}\tan^{-1}\frac{2R_{x_i y_i}(0)}{R_{x_i x_i}(0) - R_{y_i y_i}(0)} \tag{4-5}$$

The principal variance ratio $R(f_o)$ is given by

$$0 < R(f_o) = \frac{R_{y''y''}(f_o)}{R_{x''x''}(f_o)} < 1 \qquad (4\text{-}6)$$

Once the ground motion has been resolved into distinct phases at various frequencies, the variance function for a pair of time histories can be used to determine the propagation velocity. The time lag for maximum correlation between a pair of stations can be determined by maximizing the variance function with respect to τ for a pair of time histories resolved in the direction of the dominant motion. The propagation velocity is determined from the slope of a best fit line through the points plotted of time lag for maximum correlation and relative distance projected in the direction of dominant motion.

An example of the preceding analysis is presented in Ref. 14 and is repeated in Figs. 4-1 through 4-4. In Fig. 4-1 the variance function, principal variance ratio and direction of dominant motion are plotted versus frequency for three stations in a 37 station array. A predominant phase is evident for four frequencies shown in Fig. 4-1. For frequencies f_1 and f_2 the direction of dominant motion is in the direction towards the epicenter while for f_3 and f_4 the the motion is primarily normal to the epicenter direction. The calculated dominant directions for frequencies f_1 and f_3 at stations on the array are plotted in Figs. 4-2 and 4-3. Average propagation velocities are determined from Fig. 4-4 for f_1 and f_3. From the analysis of the propagation velocity and direction of dominant motion, it was concluded that the phase corresponding to f_1 was Rayleigh, while, for f_3, the wave type was a SH or Love wave. These conclusions were checked by determining the vertical motions for frequencies around f_1 and f_3.

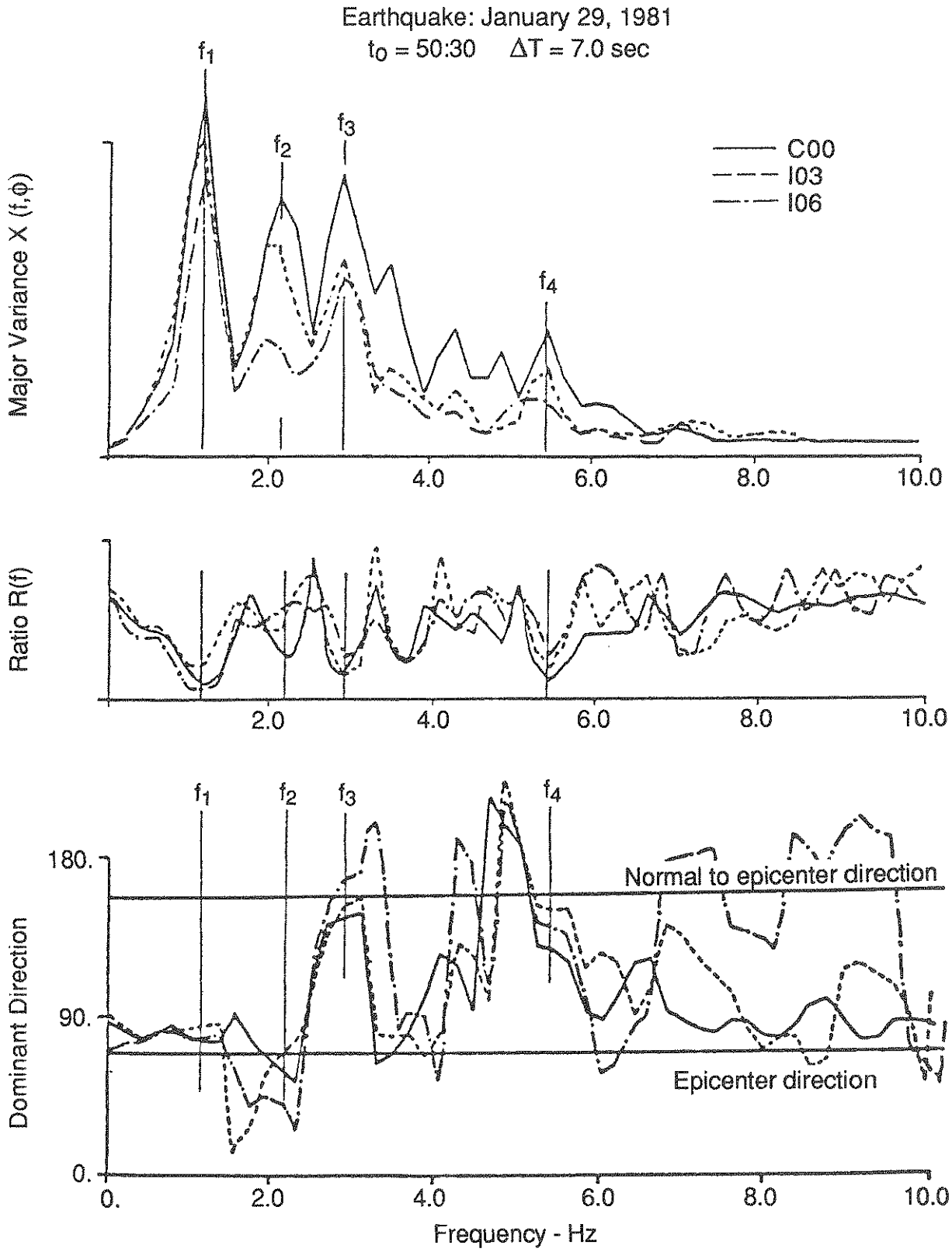

FIGURE 4-1 Major Principal Variance, Variance Ratio And Dominant Direction For Event 5, Ref. 14

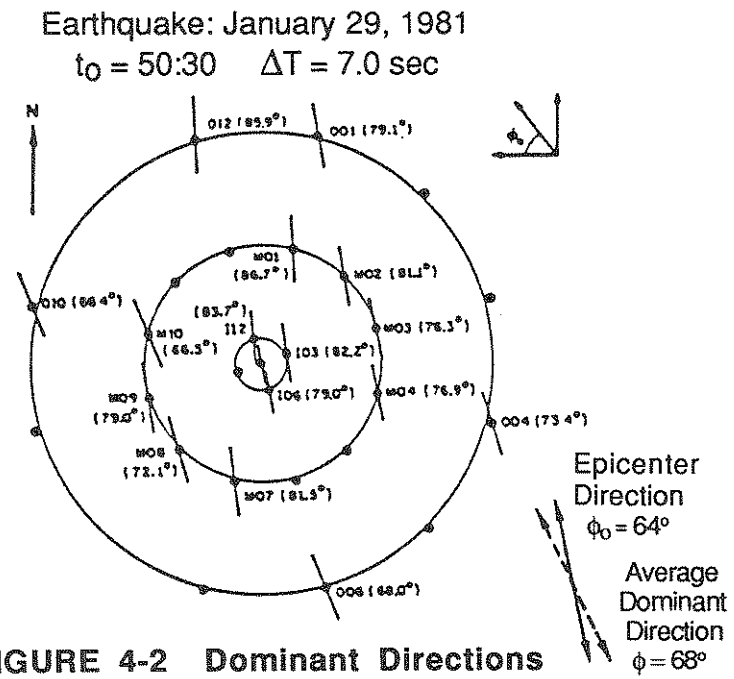

FIGURE 4-2 Dominant Directions At 1.17 Hz For Event 5

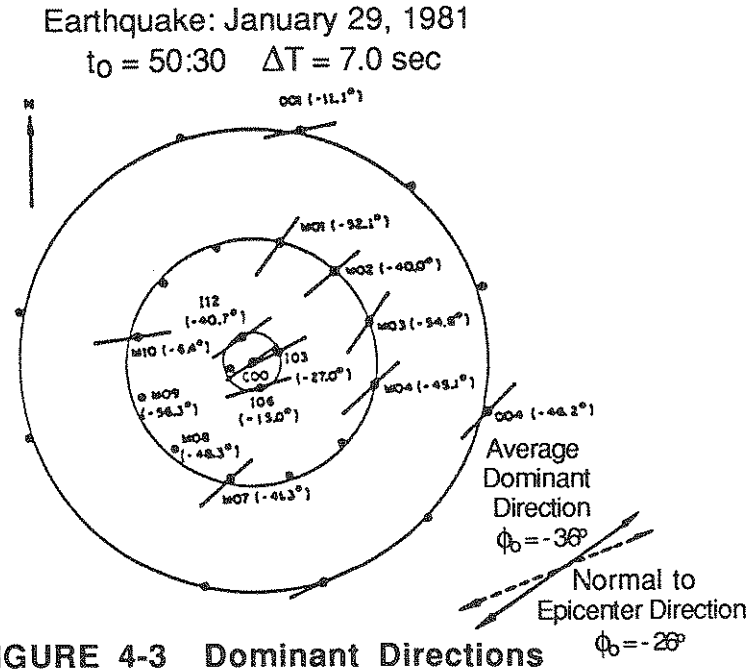

FIGURE 4-3 Dominant Directions At 2.85 Hz For Event 5

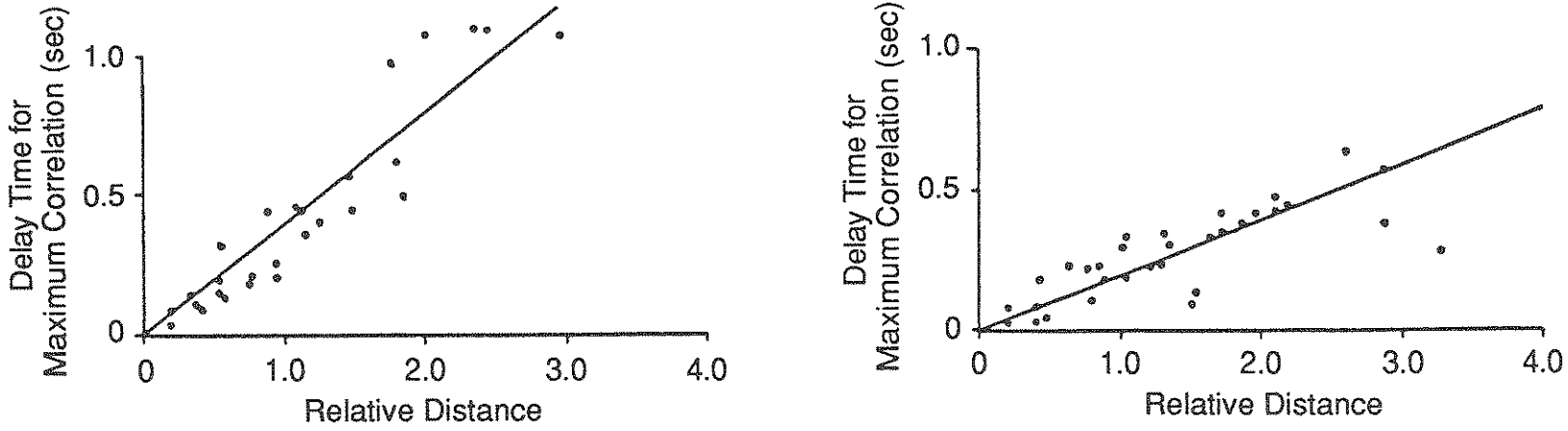

FIGURE 4-4 Identification Of Wave Velocity At Frequencies 1.17 Hz And 2.85 Hz, Ref. 14

SECTION 5
STATUS AND PLANNED FUTURE ACTIVITIES

To capitalize on potential enhancements provided by Japanese seismometers, the data acquisition rates for pipe strains and displacements need to be increased. This is planned in 1988-89.

Instability in a few strain gages is causing the data logger to trigger and record non-events that could overwrite real earthquake data in a matter of a day or so. Temperature shielding of the junction boxes (shunt cal boxes) will be tried; rewiring to eliminate shunt cal boxes completely is a possibility.

Further cooperation with Japanese workers will be explored in order to gain access to comparable Japanese data.

SECTION 6
CONCLUSIONS

Because the predicted earthquake has not yet occurred, no conclusions can be drawn regarding the validity of current models for pipe-soil interaction due to lateral offset or to ground strain induced by seismic waves. However, even before the earthquake occurs, the present experiment has value in focusing attention on the vulnerability of gas, sewer and water transmission pipelines which cross fault zones. This is demonstrated by the interest expressed by Japanese researchers at Kyoto University who have donated seismometers to the project and by a group of pipeline manufacturers and California and Oregon Utilities who have agreed to review and comment on papers and reports prepared under the project.

Based on the experience of the past 12 months, the difficulties which are inherent in automatic, remote data acquisition can be overcome with further attention given to such details as grounding and terminal connections.

SECTION 7
REFERENCES

1. Isenberg, J. and E. Richardson, "Pipeline Experiment at Parkfield, California," Technical Report NCEER-87-0016, Weidlinger Associates, 15 September 1987.

2. Isenberg, J., E. Richardson and T. D. O'Rourke, "Buried Pipelines Across San Andreas Fault," 9th World Conf. on Earthquake Engineering, Tokyo-Kyoto, August 1988.

3. Newmark, N. M. and W. J. Hall, "Pipeline Design to Resist Large Fault Displacement," Proc. U.S. National Conf. on Earthquake Engineering, Ann Arbor, Michigan, 18-20 June 1975.

4. Kennedy, R. P., A. W. Chow and R. A. Williamson, "Fault Movement Effects on Buried Oil Pipelines," J. of the Transportation Engineering Div. Proc. ASCE, Vol. 103, 1977.

5. Wang, L. R-L, "Role and Development of Soil Parameters for Seismic Response of Buried Lifelines," Proc. of the 4th National Congress on Pressure Vessel and Piping Technology, Earthquake Behavior and Safety of Oil and Gas Storage Facilities, Buried Pipelines and Equipment, ASME PVP 77, Portland, Oregon, June 1983.

6. Takada, S. "Experimental Study on Mechanical Behavior of PVC Pipelines Subjected to Ground Subsidence," Proc. of the 4th National Congress on Pressure Vessel and Piping Technology , Earthquake Behavior and Safety of Oil and Gas Storage Facilities, Buried Pipelines and Equipment, ASME PVP 77, Portland, Oregon, June 1983.

7. Trautmann, C. H. and T. D. O'Rourke, "Load-Displacement Characteristics of A Buried Pipe Affected by Permanent Earthquake Ground Movements," Proc. of the 4th National Congress on Pressure Vessel and Piping Technology, Earthquake Behavior and Safety of Oil and Gas Storage Facilities, Buried Pipelines and Equipment, ASME PVP 77, Portland, Oregon, June 1983.

8. Kuesel, T. R., "Earthquake Design Criteria for Subways," J. of the Structural Div. Proc. ASCE, Vol. 95, No. ST6, June 1969, p. 1212-1231.

9. O'Rourke, M. J., G. Castro and I. Hossain, "Horizontal Soil Strain Due to Seismic Waves," J. of Geotechnical Eng., Vol. 110. No. 9, September 1984, p. 1173-1187.

10. Shinozuka, M. R., Y. Tan and T. Koike, "Serviceability of Water Trans- mission Systems Under Seismic Risk," Proc. of the 2nd Specialty Conf. of the Tech. Council on Lifeline Earthquake Eng. ASCE, August 1981.

11. Shinozuka, M. and T. Koike, "Estimation of Structural Strains in Underground Lifeline Pipes," Technical Report No. NSF-PFR-78-15049-CU-4, Dept. of Civil Engineering and Engineering Mechanics, Columbia University, March 1979.

12. Datta, S. K., A. H. Shah and N. El-Akily, "Dynamic Behavior of a Buried Pipe in a Seismic Environment," J. of Applied Mechanics, Trans. ASME, Vol. 49, 1982, p. 141-148.

13. Kawashima, K., Public Works Research Institute, Ministry of Construction, Government of Japan, Private Communication, 16 July 1987.

14. Loh, C. H. and J. Penzien, "Identification of Wave Types, Directions and Velocities Using SMART-1 Strong Motions Array Data," Proc. of the 8th World Conf. on Earthquake Engineering, Vol II, San Francisco 1984, p. 191-198.

15. Wilmesher, J. F., geologist, USGS, personal communication addressed to E. Richardson, 25 May 1988.

16. American Society for Testing and Materials, "Standard Methods of Tension Testing of Metallic Materials (ASTM E8-85b)," Volume 03.01, ASTM, Philadelphia, Pennsylvania, 1986, p. 124-145.

17. O'Rourke, T.D., "Evaluation of Pipeline and Soil-Pipe Interface Shear Characteristics for the Owen's Pasture Test Site," Report No. 88-WEID-01, April 1988.

18. Potyondy, J. G., "Skin Friction Between Various Soils and Construction Materials," Geotechnique, Vol. 11, No. 2, December 1961, pp. 339-353.

19. Kulhawy, F. H. and M. S. Peterson, "Behavior of Sand-Concrete Interfaces," Proc., 6th Pan American Conf. on Soil Mechanics and Foundation Engineering, Vol. 2, Lima, December 1979, p. 225-236.

20. Iwasaki, T., "Earthquake Resistant Design of Underground Pipelines in Japan," Proc. of the US-Japan Workshop on Seismic Behavior of Buried Pipelines and Telecommunications Systems, Tsukuba Science City, Japan, 5-7 December 1984.

21. O'Rourke, T. D., M. Grigoriu and M. Khater, "Seismic Response of Buried Pipelines," Pressure Vessel and Piping Technology - A Decade of Progress, C. Sundararajan, Ed., ASME, New York, New York, 1985, pp. 281-323.

22. Committee on Gas and Liquid Fuel Lifelines, "Guidelines for the Seismic Design of Oil and Gas Pipeline Systems," ASCE, New York, NY , 1984.

APPENDIX A
WIDE RANGE DIGITAL SEISMOGRAPH
MODEL SAMTAC-17

The SAMTAC-17 is newly developed wide range digital seismograph which consists of a high sensitivity seismometer, amplifier and digital data recorder. This instrument is manufactured by Tokyo Sokushin Co., Ltd., of Tokyo, Japan.

The recording unit in the present system consists of a digital magnetic tape system. This unit has a digital data delay memory, a crystal time clock with automatic revision, a versatile triggering circuit and a D/A converter for monitoring. The magnetic data tapes can be easily read using your host computer.

SAMTAC-17S

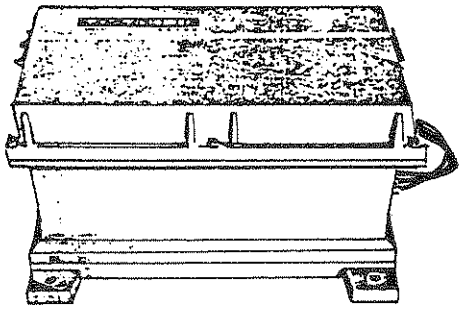

Case: Water Proof

SAMTAC-17E

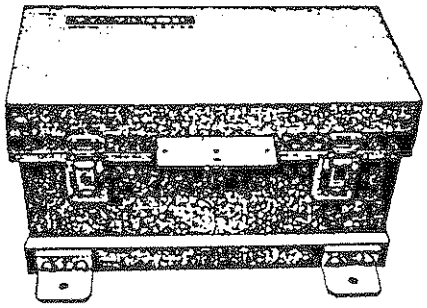

Case: Water Resistant

SPECIFICATIONS

Sensor	Force balance accelerometer
Channels	Triaxial, internal
Recording range	± 1000 gal @ .03 gal resolution
Frequency range	0.05 Hz ≈ 30 Hz
A/D converter	16 bit binary
Sampling frequency	200 Hz
Pre-event memory	5 sec
Crystal clock	Calender clock - Month, day, hour, minute and second are represented.
Trigger circuit	
Trigger component	Selectable: X, Y or Z
Trigger level	0 to 20% of full scale
Duration of recording	Recording continues next 30 seconds after the signal falls below a specified level.
Countermeasure for noise	Software is used to distinguish between noise and earthquake.
Recording time	About 30 minutes; 450 ft tape
Magnetic tape	3M Cartridge tape ANSIX 3.55-1977
D/A converter	Analog monitoring is possible in record or playback mode
Shock	
Horizontal	Max. 3 g
Vertical	Max. 0.5 g
Power requirement	
Voltage	100 Vac
Power	Average 30 VA

APPENDIX B
NEWMARK-HALL MODEL OF FAULT CROSSING

1. Assume tensile elongation for pipeline crossing:

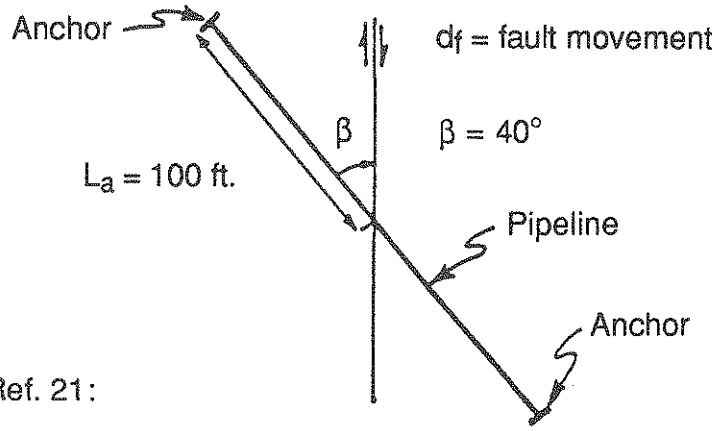

Let:
σ = max stress in pipe
σ_{an} = stress at anchor
σ_0, σ_1, ε_1, E_1, and E_2
as defined in Fig. 3-6

from Ref. 21:

when $0 < \sigma_{an} < \sigma_1$

$$\frac{\sigma - 2\sigma_0 + \sigma_1}{2E_2} = \frac{f}{2(\sigma - \sigma_1)}\left(\frac{d_f}{t}\right)\cos\beta + \frac{f^2}{8(\sigma - \sigma_{an})(\sigma - \sigma_1)}\left(\frac{d_f}{t}\right)^2 \sin^2\beta - \frac{(\sigma - \sigma_{an})(\sigma + \sigma_{an})}{2E_1(\sigma - \sigma_1)} \qquad \text{(B-1)}$$

2. Determine f:

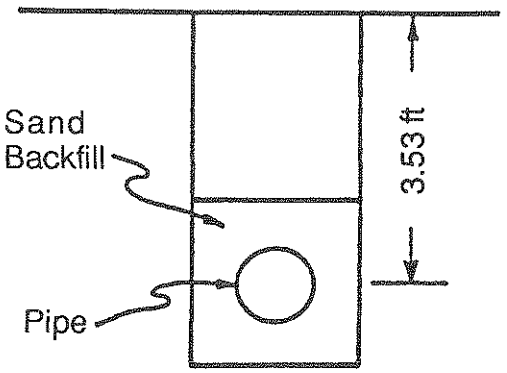

D_p = 12.75 in OD
t = 0.125 in

Assume:
Dry unit of wt sand, γ_d = 105 pcf from Fig. 3-11, δ = 25°. Also, partially saturated unit weight, γ = 115 pcf

$$f = \left(\frac{1+k_o}{2}\right)(115 \text{ pcf})(3.5 \text{ ft})\tan\delta$$

f = 142 psf = 0.99 psi

3. Determine σ:

Note: $\sigma - \sigma_{an} = \frac{L_a f}{t}$

substituting into eq. (B-1), leads to:

$$\left(\sigma - 2\sigma_0 + \sigma_1\right)\left(\sigma - \sigma_1\right)\frac{L_a f}{t} - E_2\, d_f \left(\frac{f}{t}\right)^2 L_a \cos\beta - \frac{E_2}{4}\left(\frac{f}{t}\right)^2 d_f^2 \sin^2\beta + \frac{E_2}{E_1}\left[\sigma_1^2\left(\sigma - \frac{L_a f}{t}\right)\right]\frac{L_a f}{t} = 0 \qquad \text{(B-2)}$$

Solving Eq. (B-2) using the trilinear representation in Fig. 3-6 for

$d_f = 4$ in , assumed fault offset

$L_a = 100$ ft, assumed anchor length

leads to $\sigma = 39.8$ ksi

4. Evaluate ε_{max}:

$$\sigma_{an} = \sigma - \frac{L_a f}{t}$$

$$\sigma_{an} = 39.8 \text{ ksi} - \left(\frac{0.99 \text{ psi}}{0.125 \text{ in}}\right)(100 \text{ ft})\left(\frac{12 \text{ in}}{1 \text{ ft}}\right)$$

$\sigma_{an} = 30.3$ ksi $< \sigma$, so checks

$$\varepsilon_{max} = \frac{\sigma - \sigma_0}{E_2} = \frac{39.8 \text{ ksi} - 26 \text{ ksi}}{7.78 \times 10^3 \text{ ksi}}$$

$\varepsilon_{max} = 0.18\%$ the extensional strain in the pipe

APPENDIX C
KENNEDY ET AL MODEL OF FAULT CROSSING

For Kennedy et al. model, use same geometry, soil and pipeline properties as in steps 1 and 2 of Appendix B, and adopting notation similar to that in Ref. 22, proceed as follows:

1. Estimate Q:

$$Q = \sigma A_s \tag{C-1}$$

From Newmark and Hall analysis, σ = 39.8 ksi. From this and inspection of Ramberg-Osgood formulation in Fig. 3-7,

Choose σ = 43 ksi

A_S = 4.96 in^2 = x-sect area of pipe

Q = 43 ksi (4.96 in^2) = 213.3 kips

2. Determine Pipeline Elongation, ΔL_R:

$$\Delta L_R = d_f \cos\beta + \frac{d_f^2 \sin^2\beta}{3L_{cl}} \tag{C-2}$$

$$L_{cl} = \left(d_f \sin\beta \, R_{cl}\right)^{\frac{1}{2}} \tag{C-3}$$

$$R_{CL} = \frac{Q}{p_u}\text{; } p_u = \text{lateral soil force per unit distance} \tag{C-4}$$

from p. 167 in Ref. 22, for $\frac{H}{D_p} = \frac{42.7 \text{ in.}}{12.75 \text{ in.}} = 3.3$ and $\phi = 35°$

$N_{qh} = 6.5$

$p_u = N_{qh}\ \gamma\ HD_p$

$p_u = 6.5\ (115 \text{ pcf})(3.53 \text{ ft})(1.06 \text{ ft}) = 2.80$

so,

$$R_{CL} = \frac{213.3 \text{ k}}{2.80 \frac{\text{k}}{\text{ft}}} = 76.2 \text{ ft}$$

and,

$$L_{cl} = \left[4 \text{ in}\left(\frac{1 \text{ ft}}{12 \text{ in.}}\right)\sin 40° \ (76.2 \text{ ft})\right]^{\frac{1}{2}} = 4.04 \text{ ft} \cong 4.0 \text{ ft}$$

and,

$$\Delta L_R = (0.25 \text{ ft}) \cos 40° + \frac{(0.25 \text{ ft})^2 \sin^2 (40°)}{3(4.04 \text{ ft})}$$

$\Delta L_R = 0.259$ ft: this represents total elongation of pipeline to accommodate a 4 in. fault offset.

3. Determine Elongation from Pipeline Strains:

$$\Delta L_a = 2\left(\Delta L_s + \Delta L_c\right) \tag{C-5}$$

where

$$\Delta L_s = \varepsilon_o \left\{L_s \left(\frac{B_s + B_1}{2}\right) + \frac{C}{h_s(r+2)}\left(B_s^{r+2} + B_1^{r+2}\right)\right\} \tag{C-6}$$

and

$$\Delta L_c = \varepsilon_o \left\{ L_{cl} \left(\frac{B_m + B_s}{2} \right) + \frac{C}{h_c (r+2)} \left(B_m^{r+2} + B_s^{r+2} \right) \right\} \qquad \text{(C-7)}$$

and

$\varepsilon_o = \dfrac{\sigma_E}{E_1}$ as defined in Fig. 3-7

$$\varepsilon_o = \frac{45 \text{ ksi}}{3 \times 10^4 \text{ ksi}} = 0.0015$$

$C = \dfrac{\alpha}{r+1}$, as defined in Fig. 3-7

$$C = \frac{5.5}{16.5 + 1} = 0.314$$

$h_c = \dfrac{3.3 f \pi D_p}{A_s \sigma_E}$; assume 3.3 f in zone of pipe curvature as per Ref. 4

$$h_c = \frac{3.3 \text{ (142 psf) } \pi \text{ (1.06 ft)}}{(4.96 \text{ in}^2)(45 \text{ ksi})} = 0.0069 \text{ ft}^{-1}$$

$$h_s = \frac{f \pi D_p}{A_s \sigma_E} = \frac{h_c}{3.3} = 0.0022 \text{ ft}^{-1}$$

$L_s = 100 \text{ ft} - L_{cl} = 96 \text{ ft}$

$$B_m = \frac{\sigma}{\sigma_E} = \frac{43 \text{ ksi}}{45 \text{ ksi}} = 0.955$$

$B_s = B_m - h_c L_{cl} = 0.927$

$B_1 = B_s - h_s L_s = 0.724$

---

from which,

$\Delta L_s = 0.122$ ft ; $\Delta L_c = 0.006$ ft

so,

$\Delta L_a = 2(0.122 \text{ ft} + 0.006 \text{ ft}) = 0.256$ ft

check

$\Delta L_a = L_R$

0.256 ft $\cong$ 0.259 ft; in agreement by 1% therefore estimated $\sigma = 43$ ksi is good.

4. Determine ε_a, Maximum Axial Strain in Pipe:

from Ramberg-Osgood formulation for steel;

$$\varepsilon_a = \frac{\sigma}{E_1}\left[1 + \frac{\alpha}{r+1}\left(\frac{\sigma}{\sigma_E}\right)^r\right]$$

$$\varepsilon_a = \frac{43 \text{ ksi}}{3 \times 10^4 \text{ ksi}}\left[1 + \frac{5.5}{16.5 + 1}\left(\frac{43 \text{ ksi}}{45 \text{ ksi}}\right)^{16.5}\right]$$

$\varepsilon_a = 0.164\%$ max. axial strain in pipe

5. Determine ε_b, Maximum Bending Strain in Pipe:

$$\varepsilon_b = \frac{D_p}{2} R_{CL}^{-1}$$

$$\varepsilon_b = \left(\frac{1.06 \text{ ft}}{2}\right)(76.2 \text{ ft})^{-1}$$

$\varepsilon_b = 0.69\%$ max. bending strain in pipe

6. Determine ε_T, Maximum Combined Strain in Pipe:

$$\varepsilon_T = \varepsilon_a \overset{+}{-} \varepsilon_b$$

$$\varepsilon_{max} = 0.86\%$$

NATIONAL CENTER FOR EARTHQUAKE ENGINEERING RESEARCH
LIST OF PUBLISHED TECHNICAL REPORTS

The National Center for Earthquake Engineering Research (NCEER) publishes technical reports on a variety of subjects related to earthquake engineering written by authors funded through NCEER. These reports are available from both NCEER's Publications Department and the National Technical Information Service (NTIS). Requests for reports should be directed to the Publications Department, National Center for Earthquake Engineering Research, State University of New York at Buffalo, Red Jacket Quadrangle, Buffalo, New York 14261. Reports can also be requested through NTIS, 5285 Port Royal Road, Springfield, Virginia 22161. NTIS accession numbers are shown in parenthesis, if available.

NCEER-87-0001 "First-Year Program in Research, Education and Technology Transfer," 3/5/87, (PB88-134275/AS).

NCEER-87-0002 "Experimental Evaluation of Instantaneous Optimal Algorithms for Structural Control," by R.C. Lin, T.T. Soong and A.M. Reinhorn, 4/20/87, (PB88-134341/AS).

NCEER-87-0003 "Experimentation Using the Earthquake Simulation Facilities at University at Buffalo," by A.M. Reinhorn and R.L. Ketter, to be published.

NCEER-87-0004 "The System Characteristics and Performance of a Shaking Table," by J.S. Hwang, K.C. Chang and G.C. Lee, 6/1/87, (PB88-134259/AS).

NCEER-87-0005 "A Finite Element Formulation for Nonlinear Viscoplastic Material Using a Q Model," by O. Gyebi and G. Dasgupta, 11/2/87, (PB88-213764/AS).

NCEER-87-0006 "Symbolic Manipulation Program (SMP) - Algebraic Codes for Two and Three Dimensional Finite Element Formulations," by X. Lee and G. Dasgupta, 11/9/87, (PB88-219522/AS).

NCEER-87-0007 "Instantaneous Optimal Control Laws for Tall Buildings Under Seismic Excitations," by J.N. Yang, A. Akbarpour and P. Ghaemmaghami, 6/10/87, (PB88-134333/AS).

NCEER-87-0008 "IDARC: Inelastic Damage Analysis of Reinforced Concrete Frame - Shear-Wall Structures," by Y.J. Park, A.M. Reinhorn and S.K. Kunnath, 7/20/87, (PB88-134325/AS).

NCEER-87-0009 "Liquefaction Potential for New York State: A Preliminary Report on Sites in Manhattan and Buffalo," by M. Budhu, V. Vijayakumar, R.F. Giese and L. Baumgras, 8/31/87, (PB88-163704/AS). This report is available only through NTIS (see address given above).

NCEER-87-0010 "Vertical and Torsional Vibration of Foundations in Inhomogeneous Media," by A.S. Veletsos and K.W. Dotson, 6/1/87, (PB88-134291/AS).

NCEER-87-0011 "Seismic Probabilistic Risk Assessment and Seismic Margins Studies for Nuclear Power Plants," by Howard H.M. Hwang, 6/15/87, (PB88-134267/AS). This report is available only through NTIS (see address given above).

NCEER-87-0012 "Parametric Studies of Frequency Response of Secondary Systems Under Ground-Acceleration Excitations," by Y. Yong and Y.K. Lin, 6/10/87, (PB88-134309/AS).

NCEER-87-0013 "Frequency Response of Secondary Systems Under Seismic Excitation," by J.A. HoLung, J. Cai and Y.K. Lin, 7/31/87, (PB88-134317/AS).

NCEER-87-0014 "Modelling Earthquake Ground Motions in Seismically Active Regions Using Parametric Time Series Methods," by G.W. Ellis and A.S. Cakmak, 8/25/87, (PB88-134283/AS).

NCEER-87-0015 "Detection and Assessment of Seismic Structural Damage," by E. DiPasquale and A.S. Cakmak, 8/25/87, (PB88-163712/AS).

NCEER-87-0016 "Pipeline Experiment at Parkfield, California," by J. Isenberg and E. Richardson, 9/15/87, (PB88-163720/AS).

NCEER-87-0017 "Digital Simulation of Seismic Ground Motion," by M. Shinozuka, G. Deodatis and T. Harada, 8/31/87, (PB88-155197/AS). This report is available only through NTIS (see address given above).

NCEER-87-0018 "Practical Considerations for Structural Control: System Uncertainty, System Time Delay and Truncation of Small Control Forces," J.N. Yang and A. Akbarpour, 8/10/87, (PB88-163738/AS).

NCEER-87-0019 "Modal Analysis of Nonclassically Damped Structural Systems Using Canonical Transformation," by J.N. Yang, S. Sarkani and F.X. Long, 9/27/87, (PB88-187851/AS).

NCEER-87-0020 "A Nonstationary Solution in Random Vibration Theory," by J.R. Red-Horse and P.D. Spanos, 11/3/87, (PB88-163746/AS).

NCEER-87-0021 "Horizontal Impedances for Radially Inhomogeneous Viscoelastic Soil Layers," by A.S. Veletsos and K.W. Dotson, 10/15/87, (PB88-150859/AS).

NCEER-87-0022 "Seismic Damage Assessment of Reinforced Concrete Members," by Y.S. Chung, C. Meyer and M. Shinozuka, 10/9/87, (PB88-150867/AS). This report is available only through NTIS (see address given above).

NCEER-87-0023 "Active Structural Control in Civil Engineering," by T.T. Soong, 11/11/87, (PB88-187778/AS).

NCEER-87-0024 Vertical and Torsional Impedances for Radially Inhomogeneous Viscoelastic Soil Layers," by K.W. Dotson and A.S. Veletsos, 12/87, (PB88-187786/AS).

NCEER-87-0025 "Proceedings from the Symposium on Seismic Hazards, Ground Motions, Soil-Liquefaction and Engineering Practice in Eastern North America," October 20-22, 1987, edited by K.H. Jacob, 12/87, (PB88-188115/AS).

NCEER-87-0026 "Report on the Whittier-Narrows, California, Earthquake of October 1, 1987," by J. Pantelic and A. Reinhorn, 11/87, (PB88-187752/AS). This report is available only through NTIS (see address given above).

NCEER-87-0027 "Design of a Modular Program for Transient Nonlinear Analysis of Large 3-D Building Structures," by S. Srivastav and J.F. Abel, 12/30/87, (PB88-187950/AS).

NCEER-87-0028 "Second-Year Program in Research, Education and Technology Transfer," 3/8/88, (PB88-219480/AS).

NCEER-88-0001 "Workshop on Seismic Computer Analysis and Design of Buildings With Interactive Graphics," by W. McGuire, J.F. Abel and C.H. Conley, 1/18/88, (PB88-187760/AS).

NCEER-88-0002 "Optimal Control of Nonlinear Flexible Structures," by J.N. Yang, F.X. Long and D. Wong, 1/22/88, (PB88-213772/AS).

NCEER-88-0003 "Substructuring Techniques in the Time Domain for Primary-Secondary Structural Systems," by G.D. Manolis and G. Juhn, 2/10/88, (PB88-213780/AS).

NCEER-88-0004 "Iterative Seismic Analysis of Primary-Secondary Systems," by A. Singhal, L.D. Lutes and P.D. Spanos, 2/23/88, (PB88-213798/AS).

NCEER-88-0005 "Stochastic Finite Element Expansion for Random Media," by P.D. Spanos and R. Ghanem, 3/14/88, (PB88-213806/AS).

NCEER-88-0006 "Combining Structural Optimization and Structural Control," by F.Y. Cheng and C.P. Pantelides, 1/10/88, (PB88-213814/AS).

NCEER-88-0007 "Seismic Performance Assessment of Code-Designed Structures," by H.H-M. Hwang, J-W. Jaw and H-J. Shau, 3/20/88, (PB88-219423/AS).

NCEER-88-0008 "Reliability Analysis of Code-Designed Structures Under Natural Hazards," by H.H-M. Hwang, H. Ushiba and M. Shinozuka, 2/29/88, (PB88-229471/AS).

NCEER-88-0009 "Seismic Fragility Analysis of Shear Wall Structures," by J-W Jaw and H.H-M. Hwang, 4/30/88, (PB89-102867/AS).

NCEER-88-0010 "Base Isolation of a Multi-Story Building Under a Harmonic Ground Motion - A Comparison of Performances of Various Systems," by F-G Fan, G. Ahmadi and I.G. Tadjbakhsh, 5/18/88, (PB89-122238/AS).

NCEER-88-0011 "Seismic Floor Response Spectra for a Combined System by Green's Functions," by F.M. Lavelle, L.A. Bergman and P.D. Spanos, 5/1/88, (PB89-102875/AS).

NCEER-88-0012 "A New Solution Technique for Randomly Excited Hysteretic Structures," by G.Q. Cai and Y.K. Lin, 5/16/88, (PB89-102883/AS).

NCEER-88-0013 "A Study of Radiation Damping and Soil-Structure Interaction Effects in the Centrifuge," by K. Weissman, supervised by J.H. Prevost, 5/24/88, (PB89-144703/AS).

NCEER-88-0014 "Parameter Identification and Implementation of a Kinematic Plasticity Model for Frictional Soils," by J.H. Prevost and D.V. Griffiths, to be published.

NCEER-88-0015 "Two- and Three- Dimensional Dynamic Finite Element Analyses of the Long Valley Dam," by D.V. Griffiths and J.H. Prevost, 6/17/88, (PB89-144711/AS).

NCEER-88-0016 "Damage Assessment of Reinforced Concrete Structures in Eastern United States," by A.M. Reinhorn, M.J. Seidel, S.K. Kunnath and Y.J. Park, 6/15/88, (PB89-122220/AS).

NCEER-88-0017 "Dynamic Compliance of Vertically Loaded Strip Foundations in Multilayered Viscoelastic Soils," by S. Ahmad and A.S.M. Israil, 6/17/88, (PB89-102891/AS).

NCEER-88-0018 "An Experimental Study of Seismic Structural Response With Added Viscoelastic Dampers," by R.C. Lin, Z. Liang, T.T. Soong and R.H. Zhang, 6/30/88, (PB89-122212/AS).

NCEER-88-0019 "Experimental Investigation of Primary - Secondary System Interaction," by G.D. Manolis, G. Juhn and A.M. Reinhorn, 5/27/88, (PB89-122204/AS).

NCEER-88-0020 "A Response Spectrum Approach For Analysis of Nonclassically Damped Structures," by J.N. Yang, S. Sarkani and F.X. Long, 4/22/88, (PB89-102909/AS).

NCEER-88-0021 "Seismic Interaction of Structures and Soils: Stochastic Approach," by A.S. Veletsos and A.M. Prasad, 7/21/88, (PB89-122196/AS).

NCEER-88-0022 "Identification of the Serviceability Limit State and Detection of Seismic Structural Damage," by E. DiPasquale and A.S. Cakmak, 6/15/88, (PB89-122188/AS).

NCEER-88-0023 "Multi-Hazard Risk Analysis: Case of a Simple Offshore Structure," by B.K. Bhartia and E.H. Vanmarcke, 7/21/88, (PB89-145213/AS).

NCEER-88-0024 "Automated Seismic Design of Reinforced Concrete Buildings," by Y.S. Chung, C. Meyer and M. Shinozuka, 7/5/88, (PB89-122170/AS).

NCEER-88-0025 "Experimental Study of Active Control of MDOF Structures Under Seismic Excitations," by L.L. Chung, R.C. Lin, T.T. Soong and A.M. Reinhorn, 7/10/88, (PB89-122600/AS).

NCEER-88-0026 "Earthquake Simulation Tests of a Low-Rise Metal Structure," by J.S. Hwang, K.C. Chang, G.C. Lee and R.L. Ketter, 8/1/88, (PB89-102917/AS).

NCEER-88-0027 "Systems Study of Urban Response and Reconstruction Due to Catastrophic Earthquakes," by F. Kozin and H.K. Zhou, 9/22/88, to be published.

NCEER-88-0028 "Seismic Fragility Analysis of Plane Frame Structures," by H.H-M. Hwang and Y.K. Low, 7/31/88, (PB89-131445/AS).

NCEER-88-0029 "Response Analysis of Stochastic Structures," by A. Kardara, C. Bucher and M. Shinozuka, 9/22/88, (PB89-174429/AS).

NCEER-88-0030 "Nonnormal Accelerations Due to Yielding in a Primary Structure," by D.C.K. Chen and L.D. Lutes, 9/19/88, (PB89-131437/AS).

NCEER-88-0031 "Design Approaches for Soil-Structure Interaction," by A.S. Veletsos, A.M. Prasad and Y. Tang, 12/30/88, (PB89-174437/AS).

NCEER-88-0032 "A Re-evaluation of Design Spectra for Seismic Damage Control," by C.J. Turkstra and A.G. Tallin, 11/7/88, (PB89-145221/AS).

NCEER-88-0033 "The Behavior and Design of Noncontact Lap Splices Subjected to Repeated Inelastic Tensile Loading," by V.E. Sagan, P. Gergely and R.N. White, 12/8/88.

NCEER-88-0034 "Seismic Response of Pile Foundations," by S.M. Mamoon, P.K. Banerjee and S. Ahmad, 11/1/88, (PB89-145239/AS).

NCEER-88-0035 "Modeling of R/C Building Structures With Flexible Floor Diaphragms (IDARC2)," by A.M. Reinhorn, S.K. Kunnath and N. Panahshahi, 9/7/88.

NCEER-88-0036 "Solution of the Dam-Reservoir Interaction Problem Using a Combination of FEM, BEM with Particular Integrals, Modal Analysis, and Substructuring," by C-S. Tsai, G.C. Lee and R.L. Ketter, 12/31/88.

NCEER-88-0037 "Optimal Placement of Actuators for Structural Control," by F.Y. Cheng and C.P. Pantelides, 8/15/88.

NCEER-88-0038 "Teflon Bearings in Aseismic Base Isolation: Experimental Studies and Mathematical Modeling," by A. Mokha, M.C. Constantinou and A.M. Reinhorn, 12/5/88.

NCEER-88-0039 "Seismic Behavior of Flat Slab High-Rise Buildings in the New York City Area," by P. Weidlinger and M. Ettouney, 10/15/88, to be published.

NCEER-88-0040 "Evaluation of the Earthquake Resistance of Existing Buildings in New York City," by P. Weidlinger and M. Ettouney, 10/15/88, to be published.

NCEER-88-0041 "Small-Scale Modeling Techniques for Reinforced Concrete Structures Subjected to Seismic Loads," by W. Kim, A. El-Attar and R.N. White, 11/22/88.

NCEER-88-0042 "Modeling Strong Ground Motion from Multiple Event Earthquakes," by G.W. Ellis and A.S. Cakmak, 10/15/88, (PB89-174445/AS).

NCEER-88-0043 "Nonstationary Models of Seismic Ground Acceleration," by M. Grigoriu, S.E. Ruiz and E. Rosenblueth, 7/15/88.

NCEER-88-0044 "SARCF User's Guide: Seismic Analysis of Reinforced Concrete Frames," by Y.S. Chung, C. Meyer and M. Shinozuka, 11/9/88, (PB89-174452/AS).

NCEER-88-0045 "First Expert Panel Meeting on Disaster Research and Planning," edited by J. Pantelic and J. Stoyle, 9/15/88, (PB89-174460/AS).

NCEER-88-0046 "Preliminary Studies of the Effect of Degrading Infill Walls on the Nonlinear Seismic Response of Steel Frames," by C.Z. Chrysostomou, P. Gergely and J.F. Abel, 12/19/88.

NCEER-88-0047 "Reinforced Concrete Frame Component Testing Facility - Design, Construction, Instrumentation and Operation," by S.P. Pessiki, C. Conley, T. Bond, P. Gergely and R.N. White, 12/16/88, (PB89-174478/AS).

NCEER-89-0001 "Effects of Protective Cushion and Soil Compliancy on the Response of Equipment Within a Seismically Excited Building," by J.A. HoLung, 2/16/89.

NCEER-89-0002 "Statistical Evaluation of Response Modification Factors for Reinforced Concrete Structures," by H.H-M. Hwang and J-W. Jaw, 2/17/89.

NCEER-89-0003 "Hysteretic Columns Under Random Excitation," by G-Q. Cai and Y.K. Lin, 1/9/89.

NCEER-89-0004 "Experimental Study of 'Elephant Foot Bulge' Instability of Thin-Walled Metal Tanks," by Z-H. Jia and R.L. Ketter, 2/22/89.

NCEER-89-0005 "Experiment on Performance of Buried Pipelines Across San Andreas Fault," by J. Isenberg, E. Richardson and T.D. O'Rourke, 3/10/89.